Neuroscience

An Anatomical and Physiological Basis for Flexible Coincidence Detection in the Auditory System

Lauren J Kreeger, Suraj Honnuraiah, Sydney Maeker, Siobhan Shea, Gord Fishell, Lisa V Goodrich

Harvard Medical School, Department of Neurobiology, Boston, USA • Stanley Center for Psychiatric Research, Broad Institute of MIT and Harvard, Cambridge, USA

Reviewed Preprint
v2 • January 7, 2025
Revised by authors

Reviewed Preprint
v1 • September 11, 2024

eLife Assessment

Kreeger et al. **convincingly** demonstrate that octopus cells in the mouse cochlear nucleus, previously thought to rely primarily on excitatory inputs for coincidence detection, also receive glycinergic inhibitory synaptic inputs that influence their synaptic integration. Using advanced techniques, including genetic mouse models, optogenetics, microscopy, slice physiology, and computational modeling, this **important** study reveals that inhibition can shunt synaptic currents and alter the timing of dendritic EPSPs, both of which are significant for auditory processing. This research broadens the understanding of octopus cells' roles in sensory processing, highlighting the importance of inhibitory inputs in shaping fast, high-frequency neural response capabilities.

https://doi.org/10.7554/eLife.100492.2.sa3

Abstract

Animals navigate the auditory world by recognizing complex sounds, from the rustle of a predator to the call of a potential mate. This ability depends in part on the octopus cells of the auditory brainstem, which respond to multiple frequencies that change over time, as occurs in natural stimuli. Unlike the average neuron, which integrates inputs over time on the order of tens of milliseconds, octopus cells must detect momentary coincidence of excitatory inputs from the cochlea during an ongoing sound on both the millisecond and submillisecond time scale. Here, we show that octopus cells receive inhibitory inputs on their dendrites that enhance opportunities for coincidence detection in the cell body, thereby allowing for responses both to rapid onsets at the beginning of a sound and to frequency modulations during the sound. This mechanism is crucial for the fundamental process of integrating the synchronized frequencies of natural auditory signals over time.

Introduction

Perception depends on the ability of neurons to encode discrete features of the sensory environment. To generate accurate percepts of complex auditory stimuli, neurons must compute both what frequencies are present and when those frequencies occur across multiple time scales. For instance, overlapping sounds, such as two competing speakers in a noisy room, are distinguished perceptually by correctly binding frequencies with coherent onsets and synchronized temporal modulations[1,2]. Such computations require coincidence detection that can encode co-occurring frequencies with submillisecond precision. Frequency information is communicated by spiral ganglion neurons (SGNs), whose central axons, also called auditory nerve fibers, project through the eighth nerve, bifurcate, and spread tonotopically to fill each division of the cochlear nucleus complex (CNC)[3–7] (**Fig. 1A**). In addition, SGNs fall into physiologically distinct subtypes that are recruited at different intensities, allowing sounds to be detected across a wide dynamic range [8–14]. Many target neurons receive SGN inputs from a limited range of frequencies, encoding only a fraction of the frequency components within a stimulus. This presents a challenge for auditory circuits which must ultimately bind co-occurring frequencies while retaining sequence information in order to locate and recognize sounds. Understanding how these first computations are made is a key step towards deciphering the basis of perception.

In the mammalian auditory system, precise encoding of broadband timing information begins with the octopus cells of the CNC. Octopus cells are excitatory neurons that bind together co-occurring frequency information on a submillisecond timescale and send this information along one of the parallel ascending pathways in the auditory brainstem. Octopus cells are named for their large-diameter tentacle-like dendrites[15,16], which are oriented unidirectionally across a tonotopic array of SGNs such that each neuron integrates inputs from a wide range of frequencies[17–20]. SGNs provide the major excitatory inputs onto octopus cells. Biophysically, octopus cells have low input resistances near rest (~4MΩ)[21,22], fast time constants (~200μs)[21–23], and large low-voltage-activated potassium (~40nS at rest)[21,23] and hyperpolarization activated (~62nS at rest)[21,22] conductances. Together these properties give octopus cells impressively narrow windows of coincidence detection on the order of 1 millisecond[24–28]. This combination of receiving SGN innervation from broad frequencies and their biophysical specializations establish octopus cells as spectrotemporal coincidence detectors that can reliably encode the timing of complex stimuli, such as the broadband transients found in speech and other natural sounds[21,29,30]. Fittingly, *in vivo* recordings from octopus cells demonstrate their ability to phase lock to broadband transients at rates up to 1kHz[31–33]. Moreover, computational models of octopus cells demonstrate that onset responses are governed by the cell's biophysical specializations and are, in large part, the result of temporal summation of excitation[34–40]. The simplicity of its connectivity combined with the precision of its temporal computations makes the octopus cell an attractive model for understanding how specialized anatomical and electrophysiological properties contribute to neuronal computations.

Although the octopus cell's integration of SGN inputs within a narrow time frame enables exceptional coincidence detection, such a model does not explain how other temporal features of sound stimuli are encoded. Indeed, octopus cells encode spectrotemporal sequences within their broadly-tuned response areas, like frequency modulated sounds, that likely require further circuit specializations[41]. Although somatic depolarization can be sufficient to activate an octopus cell[35], the vast majority of synapses are found on dendrites. Further, SGN inputs are organized tonotopically along octopus cell dendrites, with inputs from high frequency regions located more distal than those from low frequency regions. Dendritic morphology, passive cable properties, active resting membrane properties, and the spatial relationship between synaptic inputs can all impact excitatory post synaptic potential (EPSP) summation as excitation sweeps across the dendritic arbor and towards the soma. This raises the possibility that computations made in the

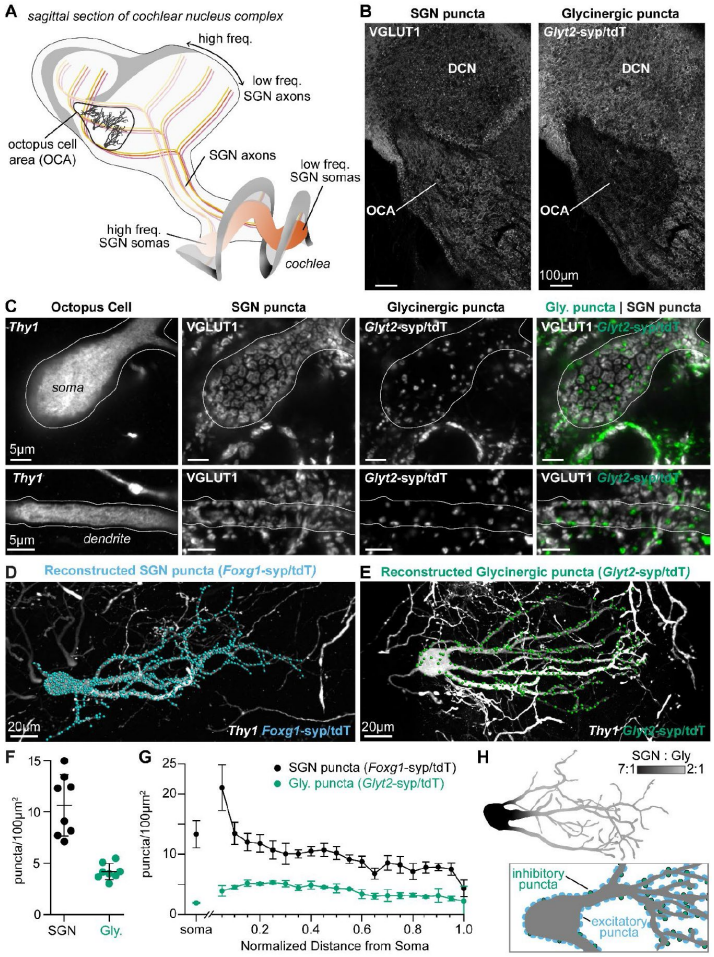

Figure 1.

Excitatory and inhibitory synapses to octopus cells form two domains.

(A) Illustration of spiral ganglion neuron (SGN) central axons branching within a parasagittal section of the mouse cochlear nucleus complex (CNC). SGN somas in the cochlea are tonotopically organized according to frequency. Axons remain organized throughout the ventral (VCN) and dorsal (DCN) divisions of the CNC. Octopus cells (inset) are found in the octopus cell area (OCA) of the VCN. **(B)** Excitatory SGN puncta labeled with a VGLUT1 antibody (left) and glycinergic puncta labeled with *Glyt2*^{Cre}-dependent syp/tdT (*Glyt2*-syp/tdT; right) in a parasagittal section of the CNC. The teardrop-shaped OCA is not devoid of inhibitory inputs, although they are less prominent than in the surrounding CNC. **(C)** A *Thy1* sparsely labeled octopus cell with excitatory SGN (VGLUT1) and inhibitory (*Glyt2*-syp/tdT) puncta. Micrographs of 3µm confocal z-stacks show puncta on the medial surface of a soma (top) and a dendrite (bottom). **(D)** Representative reconstruction of excitatory SGN puncta labeled with *Foxg1*^{Cre}-dependent syp/tdT (*Foxg1*-syp/tdT; blue) onto a *Thy1* sparsely labeled octopus cell (white). **(E)** Representative reconstruction of inhibitory puncta labeled with *Glyt2*-syp/tdT (green) onto a *Thy1* sparsely labeled octopus cell (white). **(F)** Puncta density for excitatory SGN (*Foxg1*-syp/tdT; black: 10.7 ± 3.0, *n* = 8 cells, 4 mice) and glycinergic puncta (*Glyt2*-syp/tdT; green: 4.2 ± 0.8, *n* = 8 cells, 3 mice) on octopus cell dendrites. Data are presented as mean ± SD. **(G)** Puncta density on somas for excitatory SGN (black: 13.3 ± 2.2, *n* = 8 cells, 4 mice) and glycinergic puncta (green: 1.8 ± 0.1, *n* = 8 cells, 3 mice) and the density along the length of dendrites. Data are presented as mean ± SEM. **(H)** *Top:* Illustration of an octopus cell and the ratio between excitatory SGN puncta and glycinergic puncta. *Inset:* Il-lustration of an octopus cell and the relative innervation densities of excitatory SGNs (blue) and inhibitory puncta (green).

dendrites influence the effective window of coincidence detection by the octopus cell. Such mechanisms could enable flexible processing that is adaptive to the dynamics of the environment without compromising high-fidelity coincidence computations.

Here, we sought to define the circuit mechanisms that allow octopus cells to act as coincidence detectors across time scales. We generated a comprehensive anatomical and physiological map of excitatory and inhibitory synaptic inputs onto octopus cell somas and dendrites and examined how this circuit organization influences octopus cell activation. Through a combination of *in vitro* experiments and computational modeling, we show that somatic summation of excitation is shaped by dendritic inhibition. Thus, octopus cells depend on compartmentalized computations that enable preservation of timing information both at the moment of stimulus onset and within an extended window for evidence accumulation, which is fundamental for the spectrotemporal integration of natural auditory stimuli.

Results

The balance of excitatory and inhibitory synapses is different in somatic and dendritic domains

To determine the wiring pattern that drives octopus cell computations, we generated a detailed map of excitatory and inhibitory synaptic inputs (**Fig. 1**). Overall, octopus cells receive abundant excitatory VGLUT1+ innervation from SGNs[42,43] and sparse inhibitory innervation from glycinergic neurons, as visualized using the glycinergic Cre driver *Glyt2*^{Cre}and the Ai34 synaptophysin-tdTomato (syp/tdT) fusion protein reporter (**Fig. 1B**). The *Glyt2*- syp/tdT inhibitory inputs nestle between SGN inputs, especially on octopus cell dendrites (**Fig. 1C**).

Quantification of the number and distribution of presynaptic puncta onto octopus cells revealed marked differences in the ratio of excitation and inhibition in the somatic and dendritic compartments. Since innervation patterns have never been systematically analyzed, we made three-dimensional reconstructions of 16 octopus cells and their excitatory SGN (n = 8 cells, 4 mice) and inhibitory (n = 8 cells, 3 mice) inputs. Octopus cells were visualized using a *Thy1* reporter and presynaptic puncta were labeled with the syp/tdT reporter driven either by *Foxg1*^{Cre}(**Fig. 1D**) or *Glyt2*^{Cre} (**Fig. 1E**). Consistent with qualitative assessment, the density of SGN inputs was higher (10.7 ± 3.0 SGN puncta/100μm^2) than that of inhibitory inputs (4.2 ± 0.8 puncta/100μm^2, **Fig. 1F**). Moreover, the relative proportions of excitatory and inhibitory inputs differed in the soma and dendrites (**Fig. 1G**). On somas, SGNs provided dense innervation that continued on the proximal dendrite, then gradually declined with distance from the soma. By contrast, somas received very few inhibitory inputs. On dendrites, inhibitory puncta were evenly distributed. As a result, octopus cells have a strikingly different average ratio of excitatory and inhibitory puncta on the soma (7:1) and on the dendrite (5:2), suggesting that each compartment contributes differentially to the final computation made by the octopus cell (**Fig. 1H**).

The majority of excitatory synapses on octopus cells are from type Ia SGNs

Although uniformly glutamatergic, SGNs exhibit stereotyped physiological differences in response thresholds that could affect the nature of their inputs onto octopus cells and hence coincidence detection[5,44–46,46,47]. There are three molecularly distinct SGN subtypes, referred to as Ia, Ib, and Ic SGNs, which correlate with previously shown physiological groups[10,48–53] (**Fig. 2A**). Therefore, we further categorized excitatory inputs based on SGN subtype identity. These can be identified with the presence of *Ntng1*^{Cre}-dependent reporter expression[54] in Ib and Ic SGNs (Ib/c) and its absence in Ia SGNs[50,51,53], coupled with very low to undetectable levels of calretinin (CR-) in Ic SGNs, and moderate to high levels of calretinin (CR+, CR++) in Ib and Ia SGNs

(**Fig. 2B**). As determined using the Ai14 tdTomato (tdT) reporter, *Ntng1*^{Cre}-labeled Ib/c SGNs accounted for 60.1 ± 2.6% of the entire population, with 28.5 ± 12.2% Ib SGNs, 31.6% Ic SGNs, and 39.9 ± 2.6% Ia SGNs (**Fig. 2C**: *n* = 1599 neurons, 4 mice; mean ± SD). These proportions matched scRNA-seq estimates (**Fig. 2C**), indicating that this approach provides full coverage. SGN subtype identity was further confirmed by examining the spatial organization of SGN peripheral processes en route to the inner hair cells (IHCs) in the cochlea, with Ia processes positioned deeper than Ib and Ic processes (**Fig 2A**, **Supp. Fig. 1A-C**).

Within the ventral cochlear nucleus (VCN), where octopus cells reside, *Ntng1*^{Cre} labeling was restricted to SGN central axons (**Supp. Fig. 1D-E**). There is sparse labeling in the deep layer of the dorsal cochlear nucleus (DCN) and strong labelling throughout the thalamus, hippocampus, and cortex (**Supp. Fig. 1D-E**). It is unlikely that the *Ntng1*^{Cre} labeled cells outside of the cochlea make synapses with octopus cells. When *Ntng1*^{Cre} driven tdT is co-expressed with *Foxg1*^{Flp} driven EYFP, all tdT-labeled axons in the VCN also expressed EYFP, suggesting that all our *Ntng1*^{Cre} labeled inputs are a part of the *Foxg1*^{Flp} labeled population, which are very likely to only be from SGNs in the cochlea. Additionally, in the octopus cell area, CR+ SGN central axons were segregated from *Ntng1*-tdT labeled central axons, consistent with the moderate to undetectable levels of CR in *Ntng1*-tdT SGN somas in the periphery (**Supp. Fig. 2F**). Thus, *Ntng1*^{Cre}-driven expression of syp/tdT is an appropriate tool for mapping subtype-specific connectivity onto octopus cells. Reconstruction of *Ntng1*^{Cre}-labeled Ib/c puncta (**Fig. 2D**) demonstrated that octopus cells are dominated by inputs from Ia SGN fibers, which have the lowest response thresholds and highest rates of spontaneous activity. Octopus cell dendrites received 4.1 ± 1.0 puncta/100μm^2 from Ib/c SGNs (**Fig. 2E**, magenta: *n* = 9 cells, 5 mice; mean ± SD), accounting for 38% of the total SGN density. Given that *Ntng1*-tdT+ cells account for 60.1% of the SGN population (**Fig. 2C**, magenta), Ib/c inputs were underrepresented on octopus cells. Octopus cells receive similarly low innervation from Ic inputs (**Supp. Fig. 2G-I**: *n* = 6 cells, 2 mice), as estimated from the degree of sparse labeling of Ic axons achieved by *Myo15*^{iCre}-driven reporter expression (**Supp. Fig. 2A-F**) and the expected proportion of Ic SGNs in the ganglion (**Supp. Fig. 2F**). By contrast, Ia SGNs, which comprise ~40% of the total population (**Fig. 2C**, yellow), accounted for 62 ± 9.7% of SGN synapses on octopus cells (**Fig. 2E**, yellow: 6.6 ± 1.0 puncta/100μm^2). All three subtypes showed the same overall distribution from the soma to the distal dendrite (**Fig. 2F**). Together, excitatory and inhibitory puncta densities in the innervation maps indicate the average octopus cell receives ~1035 SGN synapses (642 Ia SGN, 393 Ib/c SGN) and ~354 inhibitory synapses. Additionally, 83% of the synapses were on the dendrites, suggesting a critical role in the octopus cell computation. Octopus cell reconstructions showed the same basic wiring patterns regardless of where each cell was positioned in the octopus cell area. The tonotopic position of all reconstructed octopus cell somas was estimated in 3D reconstructions aligned to a normalized CNC model of tonotopy[55]. Octopus cells had similar morphologies (**Supp. Fig. 3E-G**) and patterns of synaptic innervation (**Supp. Fig. 3H-M**) regardless of where they were positioned along the tonotopic axis. Thus, Ia SGN synapses are the primary inputs to both the soma and dendrites of octopus cells. Additionally, the whole-neuron wiring diagram identifies a dendritic domain where inhibitory synapses are approximately equal in number to the Ib/c excitatory synapses from the periphery.

SGN inputs to octopus cells facilitate at high stimulation frequencies

Whether or not an octopus cell responds to its inputs depends on when and how EPSPs travel to and then summate in the soma. To determine if SGN subtypes transmit information differently to their central targets, we performed *in vitro* whole-cell current clamp recordings of octopus cells (**Fig. 3A**) while using Cre-dependent Channelrhodopsin-2 (ChR2) to evoke EPSPs from all SGNs (*Foxg1*-ChR2) or only Ib/c SGNs (*Ntng1*-ChR2). Octopus cells have short action potentials (~5-15mV) that resemble their large, well-timed EPSPs[25,56]. Therefore, we evoked small EPSPs that were below spike threshold and distinguishable from action potentials using a phase plot analysis. Trains of ChR2-evoked EPSPs, ranging from 5 to 50Hz, in both the total SGN population (**Fig. 3B**,

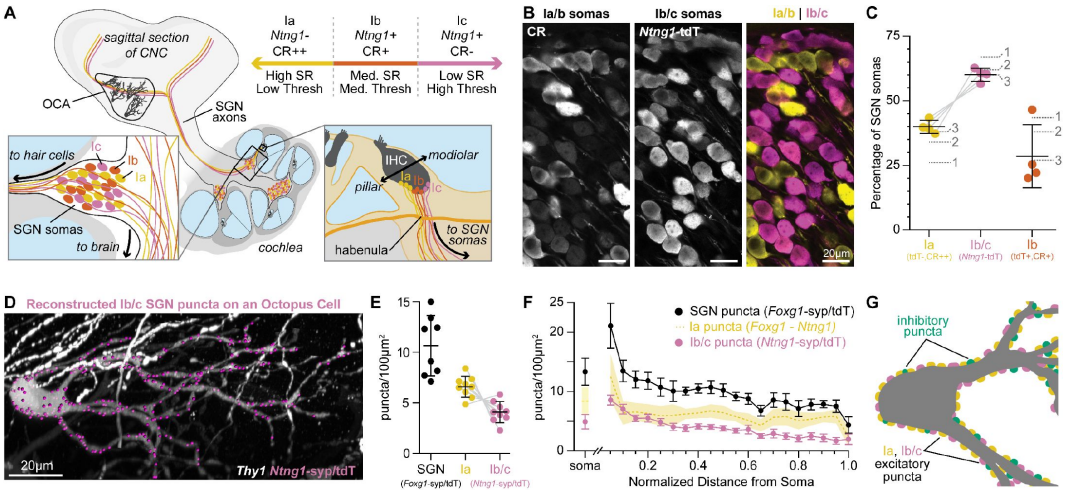

Figure 2.

Type Ia SGNs are the primary excitatory contributors to octopus cells.

(A) Ia (yellow), Ib (orange), and Ic (magenta) spiral ganglion neuron (SGN) axons innervate the cochlear nucleus complex (CNC). SGNs have a continuum of properties organized along the pillar-modiolar axis of inner hair cells (IHCs) and the habenula. *Ntng1*-expressing Ib/c fibers are positioned on the modiolar side (closest to the ganglion). Strongly calretinin immunopositive Ia fibers are on the other side (closest to the pillar cells). This organization correlates with spontaneous rates (SR) and thresholds (thresh.) measured *in vivo*. Somas of all SGN subtypes are found at all tonotopic locations. **(B)** Calretinin (CR) immunolabeling distinguishes SGN subtypes. Ia/b somas label with high (CR++) and medium (CR+) levels of CR, respectively. Ic somas label with low to undetectable levels of CR (CR-). *Ntng1*^{Cre}-mediated expression of tdT (*Ntng1*-tdT) labels Ib/c SGNs. **(C)** Ia SGNs (tdT-, CR++) make up 39.9 ± 2.6% of the SGN population. Ib/c SGNs (tdT+) make up 60.1 ± 2.6% of the SGN population. Ib SGNs (tdT+CR+) make up 28.5 ± 12.2% of the SGN population (*n* = 1599 neurons, 4 mice). Data are presented as mean ± SD; individual points represent percent coverage per animal, lines connect measurements from the same animal. Dotted lines indicate percentages from 1: Petitpré et al. 2018, 2: Shrestha et al. 2018, and 3: Sun et al. 2018. **(D)** Representative reconstruction of Ib/c puncta labeled with *Ntng1*^{Cre}-dependent syp/tdT (*Ntng1*-syp/tdT; magenta) onto a *Thy1* sparsely labeled octopus cell (white). **(E)** Puncta density for all SGNs (*Foxg1*-syp/tdT; black: data from **Fig. 1F**), Ia SGNs (*Foxg1 - Ntng1*; yellow: 6.6 ± 1.0), and Ib/c SGNs (*Ntng1*-syp/tdT; magenta: 4.1 ± 1.0, *n* = 9 cells, 5 mice) along the total dendritic length. Ia density was calculated by subtracting Ib/c density from total SGN density; lines connect measurements from the same reconstruction. Data are presented as mean ± SD. **(F)** Puncta density on somas for all SGNs (*Foxg1*-syp/tdT; black: data from **Fig. 1E**), Ia SGNs (*Foxg1 - Ntng1*; yellow: 8.4 ± 2.3), and Ib/c SNGs (*Ntng1*-syp/tdT; magenta: 4.9 ± 1.2, *n* = 9 cells, 5 mice) and the density along the length of dendrites. Data are presented as mean ± SEM. **(G)** Illustration of an octopus cell and the relative innervation densities of Ia SGNs (yellow), Ib/c SGNs (magenta), and inhibitory puncta (green).

black: *n* = 8 cells, 5 mice) and the Ib/c SGN population (**Fig. 3B**, magenta: *n* = 7 cells, 6 mice) exhibited no differences in paired-pulse plasticity at any frequency of stimulation (p > 0.35 at all interstimulus intervals, Tukey's HSD), although the Ib/c population exhibited higher variability than the total SGN population (at 20ms: SD = 0.11, SD = 0.24, respectively).

ChR2-evoked synaptic responses are known to undergo synaptic depression[57,58]. To determine if the pairedpulse depression measured in ChR2-stimulated experiments was physiological, we used electrical stimulation to evoke EPSPs from SGNs (**Fig. 3B**). Electrically-evoked EPSPs had higher paired-pulse ratios than ChR2-evoked EPSPs and were mildly facilitating at short (20ms) intervals (**Fig. 3B-C**, open circles: *n* = 5 cells, 3 mice), consistent with an octopus cell's ability to respond reliably to click trains *in vivo*[17,19,32,59]. In contrast, previous results using electrical stimulation demonstrated short-term depression of SGN inputs to octopus cells[60,61]. However, these experiments were carried out in the presence of higher, non-physiological levels of extracellular calcium. We repeated paired-pulse plasticity experiments with non-physiological calcium concentrations (2.4mM) and similarly found that electrically-evoked EPSPs from SGNs resulted in short-term depression at 50Hz of electrical stimulation (**Fig. 3C**, grey: *n* = 3 cells, 2 mice), though not to the degree observed when using full-field, ChR2-evoked inputs.

Glycine evokes inhibitory post synaptic potentials that are occluded by a low input resistance

Given the high density of inhibitory synapses on octopus cell dendrites, we considered the possibility that somatic and dendritic compartments contribute differently to the temporal computation made by octopus cells. A role for inhibition has never been incorporated into octopus cell models as previous efforts failed to reveal physiological evidence of functional inhibitory synapses either *in vitro*[25,56,62] or *in vivo*[41]. Similarly, we did not observe lightevoked (*Glyt2*-ChR2) inhibitory post synaptic potentials (IPSPs) in octopus cell somas during whole-cell current clamp recordings from P30-45 mice. Since inhibitory synapses are located primarily on octopus cell dendrites, we posited that their voltage spread to the soma is limited given the extremely low input resistance of octopus cells.

To decrease electrotonic isolation of the dendrites and increase input resistance, we pharmacologically reduced conductances from voltage-gated potassium (Kv) and hyperpolarization-activated cyclic nucleotide-gated (HCN) channels using 100μM 4-Aminopyridine (4-AP) and 50μM ZD 7288 (ZD). This cocktail increased octopus cell membrane resistance (**Fig. 4A**) and hyperpolarized the resting membrane potential ~8-10mV. To compensate for this change, membrane potentials were adjusted to within 3mV of the original resting membrane potential with a holding current. To isolate inhibition, AMPA receptor activation was blocked using 15μM 2,3-dioxo6-nitro-7-sulfamoyl-benzo[f]quinoxaline (NBQX). Consistent with our hypothesis, the increase in input resistance unveiled light-evoked IPSPs in recordings from octopus cell somas (**Fig. 4B**). Additionally, these IPSPs were fully abolished by bath application of 500nM strychnine (STN) (**Fig. 4C**), confirming the presence of functional glycinergic inhibitory synaptic transmission onto octopus cells.

To determine the types of glycinergic receptors contributing to IPSPs, we pharmacologically blocked subsets of glycine receptors (**Fig. 4C**). IPSPs were reduced upon addition of 20μM picrotoxin (PTX), which blocks homomeric glycine receptors[63–65]. Sequential addition of 100μM cyclothiazide (CTZ), which blocks α2-containing homomeric and heteromeric glycine receptors[66,67], nearly abolished the remaining IPSPs, and responses were fully abolished with further application of 500nM STN. These results indicate that relevant glycine receptors include both large conductance extrasynaptic β-subunit lacking homomeric receptors and synaptically localized α2β receptors with slower kinetics[68–70].

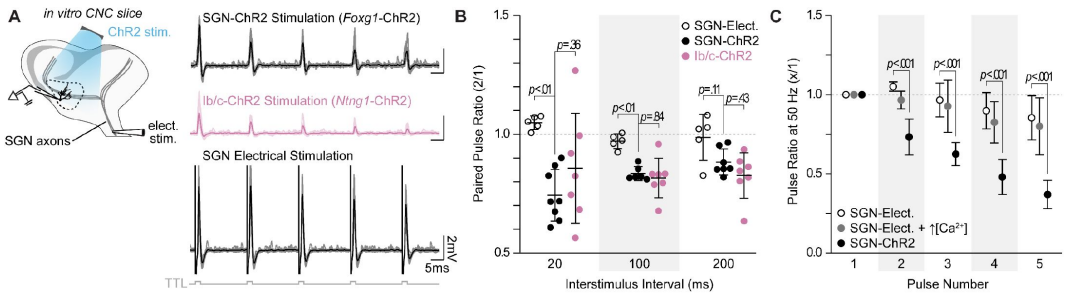

Figure 3.

SGN subtype inputs to octopus cells do not differ in short term plasticity.

(A) Illustration of the experimental paradigm and representative EPSP traces recorded during *in vitro* whole-cell current-clamp recordings of octopus cells. Spiral ganglion neuron (SGN) central axon stimulation methods included electrical stimulation or full-field, light-evoked activation of *Foxg1*- ChR2 or *Ntng1*-ChR2 SGNs. TTL trigger pulses are shown in gray. **(B)** Paired pulse ratios for electrically stimulated SGNs (open circles: n = 5 cells, 3 mice), ChR2 stimulated SGNs (*Foxg1*-ChR2; black: n = 8 cells, 5 mice), and ChR2 stimulated Ib/c SGNs (*Ntng1*-ChR2; magenta: n = 7 cells, 6 mice) at three interstimulus intervals. With electrical stimulation, SGN inputs to octopus cells were stable and exhibited slight facilitation at 50 Hz (20ms interstimulus interval). ChR2 stimulation caused paired pulse depression not seen with electrical stimulation. Data are presented as mean ± SD. Each data point represents the average paired pulse ratio for a cell. p values from ANOVA and subsequent Tukey HSD test are reported for comparisons between methods of SGN activation (electrical and ChR2) and SGN subpopulation composition within method of activation (SGN-ChR2 and Ib/c-ChR2). Welch's ANOVA was used for comparisons at 20ms interstimulus interval (50Hz) as data in this condition did not meet the homogeneity of variance assumption. **(C)** Pulse ratios at 50Hz for electrically stimulated SGNs with physiological 1.4mM Ca^{2+} ACSF (open circles: n = 5 cells, 3 mice), electrically stimulated SGNs with 2.4mM Ca^{2+} ACSF (grey: n = 3 cells, 2 mice) and ChR2 stimulated SGNs with physiological ACSF (*Foxg1*-ChR2; black: n = 8 cells, 5 mice). Data are presented as mean ± SD. $p < 0.001$ from ANOVA and subsequent Tukey HSD test for all comparisons between methods of SGN activation (electrical and ChR2). There were no statistically significant differences for all comparisons under 1.4mM and 2.4mM Ca^{2+} ($p > 0.100$, ANOVA).

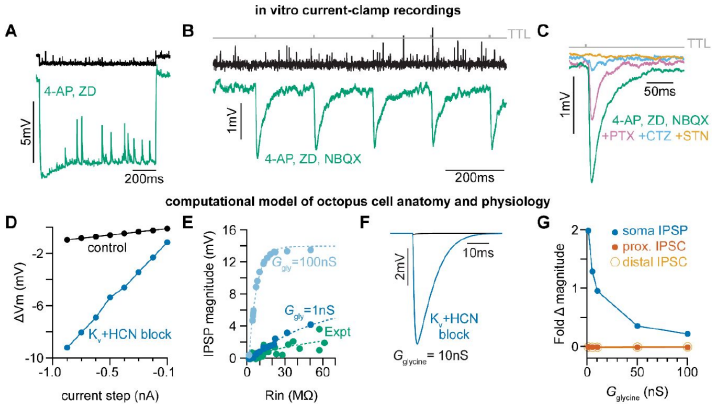

Figure 4.

Octopus cells receive glycinergic inhibitory post synaptic potentials.

(A) Voltage responses to a -200pA current injection. This representative neuron hyperpolarized 0.7mV (black) in control conditions. After bath application of 100μM 4-Aminopyridine (4-AP) and 50μM ZD 7288 (ZD), hyperpolarizing responses to the same -200pA current injection increased to 8.8mV at steady state (green). **(B)** Postsynaptic responses to ChR2 stimulation of glycinergic terminals (*Glyt2*-ChR2*)* with a 5Hz train (gray) of 1ms full-field blue light pulses before (black) and after bath application of 100μM 4-AP, 50μM ZD, and 15μM NBQX (green: *n* = 9 cells, 8 mice). Increased input resistance reveals inhibitory potentials that are difficult to detect. **(C)** Postsynaptic responses to *Glyt2*-ChR2 stimulation after bath application of 100μM 4-AP, 50μM ZD, and 15μM NBQX (green), with further sequential addition of 20μM picrotoxin (PTX, pink), 100μM cyclothiazide (CTZ, blue), and 500nM strychnine (STN, orange; *n* = 6 cells, 5 mice). **(D)** Change in membrane voltage in response to hyperpolarizing somatic current steps in a morphologically and biophysically realistic model of octopus cells before (black) and after removal of voltage-gated potassium (Kv) and hyperpolarization-activated cyclic nucleotide-gated (HCN) channels (blue). As in *in vitro* current-clamp recordings *(A)*, removing Kv and HCN channels increased the magnitude of voltage responses (ΔVm) to hyperpolarizing current. **(E)** IPSP magnitude in experimental data (green) and the model (dark and light blue) as a function of input resistance. In somatic measurements, IPSP size increases with input resistance. Modeled IPSPs are shown for two conductance levels (1nS, dark blue; 100nS light blue). **(F)** IPSPs measured at the soma of a modeled octopus cell before (black) and after removal of Kv and HCN channels (blue). As in *in vitro* current-clamp recordings, this allows for somatic IPSP detection. **(G)** Fold change in magnitude of somameasured IPSPs (blue) or dendrite-measured IPSCs at proximal (dark orange) and distal (light orange, open circles) dendritic locations after removal of Kv and HCN channels. Kv and HCN block increases the magnitude of soma-measured IPSPs. The size of dendritic IPSCs are not changed with Kv and HCN block.

To confirm whether the electrical confinement of IPSPs to the dendrites is consistent with our understanding of octopus cell biophysics, we developed an improved biophysically and anatomically accurate model of octopus cells based on our findings (**Supp. Fig. 4**)[30,71]. Passive and active properties of the model were first aligned with experimental data using a scaling factor (scl), which adjusts the maximum conductance of voltage-gated potassium (Kv) ($\bar{g}_{KLT}$, $\bar{g}_{KHT}$, $\bar{g}_{KA}$) and hyperpolarization-activated cyclic nucleotide-gated (HCN) ($\bar{g}_h$) channels (**Supp. Fig. 4A-B**). To further align the model with experimental data, we adjusted input resistance (R_N) and specific membrane resistance (R_m) to match experimentally measured input resistance under physiological conditions and with Kv and HCN block (**Supp. Fig. 4D-E**). We further examined the influence of leak, Kv, and HCN conductances on the neuron's input resistance. In a passive scenario, where leak, Kv, and HCN conductances are set to zero (g_{leak}=*0*; g_{Kv}=0; g_h=0), the input resistance scaled proportionally with specific membrane resistance (Supp. Fig F, grey). However, with active Kv and leak conductances, R_N was constrained and showed only a slight increase relative to R_m, suggesting attenuation of PSPs during their propagation to the soma (**Supp. Fig. 4F-G**). As in our current-clamp recordings (**Fig. 4A**), removal of Kv and HCN conductances in the model changed the input resistance and current-voltage relationship of the neuron, resulting in reduced electrotonic isolation (**Supp. Fig. 4C**, **Fig. 4D**, blue). We next tuned the glycine conductance (G_{gly}) to match experimental results (**Fig. 4E**). Activation of large (10nS) dendritic glycinergic conductances induced negligible hyperpolarizing voltage changes in the model (**Fig. 4F**, black). With increased input resistance and reduced electrotonic isolation, dendritic IPSPs measured at the soma were detectable, consistent with our *in vitro* recordings (**Fig. 4F**).

While blocking Kv and HCN allowed us to reveal IPSPs at the soma, it is possible that reduced electrotonic isolation does not entirely explain the increase in somaticallymeasured IPSP amplitude. Changes in driving force could increase the magnitude of synaptic currents and therefore increase the magnitude of experimentally measured synaptic potentials. We used the model to explore how changes in membrane potential under Kv and HCN block could impact the magnitude of post synaptic potentials. We simulated dendritic glycinergic conductances over a range of values and in the presence of blocked Kv and HCN channels (**Supp. Fig. 4H**). Kv and HCN block and the resulting change in input resistance increased the magnitude of somameasured IPSPs for all glycine conductances (**Fig. 4G**, blue). The size of inhibitory currents measured in the dendrites did not change as a result of the hyperpolarization induced by Kv and HCN block regardless of synaptic location on the dendrites or the magnitude of the glycine conductance (**Fig 4G**, dark orange, light orange; **Supp. Fig 4I-J**). These observations suggest that the IPSPs are difficult to detect in physiological conditions because of severe attenuation during transmission along dendrites to the soma. This is further supported by marked changes in transfer impedance (ZT), a measure of signal transmission efficiency, measured with and without Kv and HCN block (**Supp. Fig. 4K**). Together, results from the model provide evidence of functional glycinergic synaptic transmission that is difficult to detect with *in vitro* somatic recordings.

Inhibition decreases the magnitude and advances the timing of dendritic SGN inputs

SGN synapses onto octopus cell dendrites are arranged tonotopically, with higher frequency SGNs from the base of the cochlea terminating on distal dendrites and lower frequency SGNs from more apical positions terminating proximally (**Fig. 1A**). This organization has been proposed to re-synchronize coincidentally firing SGNs that are activated at slightly different times due to the time it takes for the sound stimulus to travel from the base to the apex of the cochlea[30]. To test how inhibition in the dendrites shapes coincidence detection, we first used our model to explore the influence of simultaneous activation of inhibitory and excitatory synapses at varying locations along the dendritic tree[72,73]. We modelled how somatically recorded EPSPs are affected by the location of inhibition by moving the site of excitation relative to inhibitory synapses placed either on proximal or distal dendrites (**Fig. 5A**, **Supp. Fig. 5**). In our model, inhibitory synapses that are located proximally to excitation (**Supp. Fig. 5A**) had less of an influence on excitation

recorded at the soma compared to those inhibitory synapses located distally to excitation (**Supp. Fig. 5B**). We analyzed the effect of inhibitory synapse location on somatically measured EPSPs using varying excitatory and inhibitory synaptic weight values (**Supp. Fig. 5C-F**) and determined that inhibitory conductances (G_{Gly}) between 6 and 10nS produced values within experimental ranges. For both inhibition proximal to excitation (**Fig. 5B-C**) and inhibition distal to excitation (**Fig. 5D-E**), the model predicted that inhibition reduces EPSP amplitude and accelerates EPSP peak timing at the soma. Thus, the presence of inhibition could modulate EPSP timing in dendritic compartments during continuous auditory stimuli, when inhibition can be recruited after the onset of a sound and thus allow for adaptable temporal processing during the sound's duration.

To directly test if the prediction that temporally coincident excitation and inhibition affects the timing and amplitude of excitatory SGN inputs as they travel towards the octopus cell soma, we coincidently activated SGNs and glycinergic inputs *in vitro*. In these experiments, the octopus cell properties were not altered pharmacologically and inhibition was undetectable or only visible with averaging over many sweeps (**Fig. 5F**, blue). When synaptic inhibition was evoked together with excitation (**Fig. 5F**, green), EPSPs recorded in the soma were smaller and faster than when excitation was evoked alone (**Fig. 5F**, black: n = 8 cells, 6 mice). ChR2-evoked inhibition decreased EPSP heights by 25.2 ± 9.0% (**Fig. 5G**, green) and shifted the peak of EPSPs forward 57.5 ± 26μs (**Fig. 5H**, green). This effect was mimicked by bath application of 25μM glycine (**Fig. 5G-H**, blue: n = 4 cells, 3 mice). Further, bath application of 1μM STN had the opposite effect, resulting in larger EPSPs and delayed peak times (**Fig. 5F-H**, orange: n = 5 cells, 4 mice). These findings suggest that the timing of EPSP arrival in the soma may be shaped both by tonically active glycine channels and the release of synaptic glycine onto the dendrite. Of note, many SGNs also terminate on the octopus cell soma, where inhibition is minimal. This suggests that the octopus cell's ability to act as a coincidence detector depends on two stages of compartmentalized computations, one in the dendrite that combines excitation and inhibition to provide important information about which frequencies co-occur in a complex sound stimulus and one in the soma that is restricted by the rigid temporal summation window for coincidence detection. Together with the electrotonic properties of the octopus cell and the dominance of low threshold, low jitter Ia SGN inputs, these combined computations can enable reliable coincidence detection and cross-frequency binding needed for perception of sound.

Discussion

Coincidence detection plays a critical role in many cognitive and perceptual processes, from the ability to localize sound to the binding of auditory and visual features of a common stimulus. Depending on the computation, the temporal window for integration can range widely, thereby requiring circuitry with distinct anatomical and physiological properties. Here, we describe a two-domain mechanism for coincidence detection that can detect co-occurring frequencies with different degrees of precision. By mapping and selectively activating synaptic inputs onto octopus cells both *in vitro* and in a computational model, we revealed that compartmentalized dendritic nonlinearities impact the temporal integration window under which somatic coincidence detection computations are made. The arrival of many small, reliable excitatory inputs (**Fig. 3**) rom low-threshold SGNs (**Fig. 2**) is continuous throughout an ongoing stimulus. We demonstrate that glycinergic inhibition to octopus cell dendrites (**Fig. 1**) can shift the magnitude and timing of SGN EPSPs as they summate in the soma (**Fig. 4**,**5**). The narrow window for coincidence detection computations allows the octopus cell to respond with temporal precision using momentary evidence provided by SGNs at the onset of the stimulus. We propose that, as a stimulus persists, inhibition onto octopus cell dendrites can adjust EPSPs before they arrive at the soma for the final input-output computation. This allows the cell to make an additional computation with a slightly longer window for evidence accumulation without compromising the accuracy of the somatic computation (**Fig. 6**).

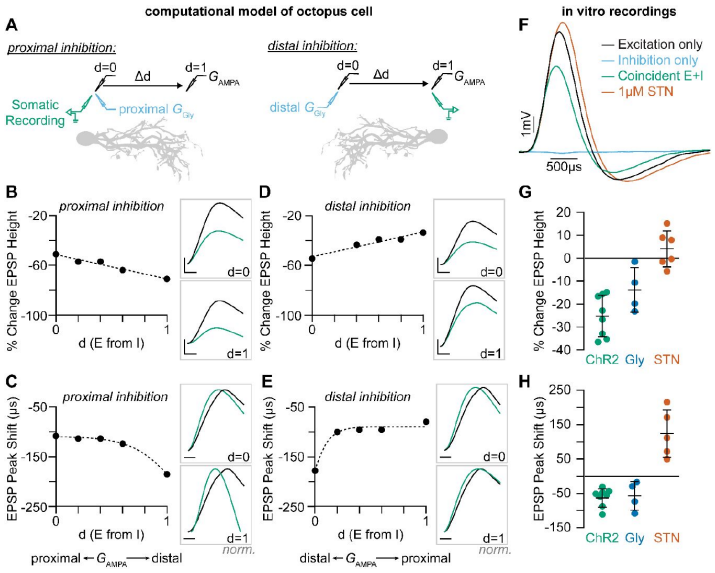

Figure 5.

Coincident excitation and inhibition on octopus cell dendrites advances EPSP peak times.

(A) The impact of distance between excitatory and inhibitory synapses was measured in a computational model of octopus cells. Inhibitory synapses were placed either proximally or distally to excitation. Excitatory synapses were placed at varying locations along the dendritic arbor to change the anatomical distance (Δd) where d=0 is the location of inhibition (G_{Gly}) and d=1 is the condition where excitation (G_{AMPA}) and inhibition are maximally separated. EPSPs were measured at the soma in all conditions (green). **(B-E)** Quantification of the percent change in soma-measured EPSP magnitude *(B, D;* G_{AMPA}=5nS*)* and the shift in EPSP peak timing *(C, E;* G_{AMPA}=2nS*)* in models of proximal *(B-C)* and distal *(D-E)* inhibition. Inhibitory conductances (G_{Gly}) between 6 and 10nS produced values within experimental ranges. Example traces show EPSPs with (green) and without (black) inhibition at d=0 and d=1. Distal dendrites (d=1) have higher local input resistance and lower IPSP attenuation due to the sealed end. Inset scale bars are 1mV, 200ms. **(F-H)** Coincident stimulation of excitation and inhibition changes EPSP shape. (*F)* Representative responses to independent stimulation of excitatory spiral ganglion neurons (SGNs; black), independent stimulation of inhibitory inputs (light blue), coincident stimulation of both excitation and inhibition (green), and independent stimulation of excitatory SGNs with the addition of 1μM strychnine (STN). Quantification of the percent change in EPSP height *(G)* and the shift in EPSP peak timing *(H)* during coincident *Glyt2*-ChR2 activation of inhibitory inputs (green: *n* = 8 cells, 6 mice), bath application of 25μM glycine (dark blue: *n* = 4 cells, 3 mice), and bath application of 1μM STN (orange: *n* = 5 cells, 4 mice). Activation of glycinergic receptors during excitation decreased EPSP heights and advanced EPSP peaks. Blocking of tonically active glycine receptors slowed and delayed EPSPs. Data are presented as mean ± SD. Markers represent the average quantification for a cell.

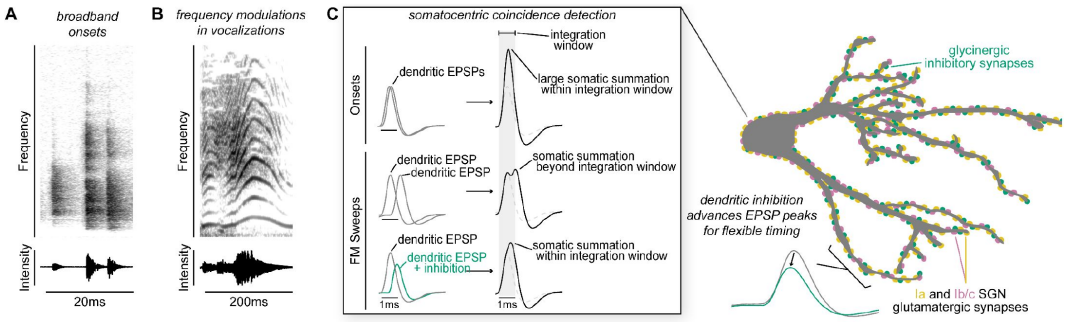

Figure 6.

Proposed model of flexible dendritic timing for precise somatic coincidence detection.

(A-B) Spectrograms show how co-occurring frequencies in broadband onsets (shown for a clicking sound, *A*) and frequency modulations (shown for human squeaking, *B*), change in their strength (top) and total intensity (bottom) on different time scales. Despite the timing differences, both kinds of stimuli are hypothesized to result in somatic summation during the octopus cell's spike integration window. **(C)** Excitation must summate at the soma of octopus cells within a narrow time window (~1ms) to achieve a depolarization rate rapid enough to trigger action potentials. Summation of excitation alone accounts for responses to sound onsets (inset, top). During stimuli that require summation over a longer time period, such as frequency modulated sweeps, synaptic inhibition can accelerate EPSPs as they travel along octopus cell dendrites towards the soma for coincidence detection computations (inset, bottom). We propose a mechanism for preferential processing of a subset of excitatory inputs where selective temporal advancement of a subset of EPSPs by local inhibition could expand the effective window for coincidence detection at the soma.

As coincidence detectors in the auditory system, octopus cells are faced with the challenge of recognizing complex sounds that include many frequencies that co-occur from the beginning to the end of the stimulus. As shown *Flexible Coincidence Detection in the Auditory System* by *in vivo* recordings[18,41], octopus cells respond well to cues that include complex spectrotemporal patterns, including frequency modulations beyond the onset of the stimulus[41]. Given that the auditory environment is filled with overlapping sound stimuli, such responses presumably allow the octopus cell to encode which frequencies belong to which sound. Our data thus support the role of octopus cells beyond simple onset coincidence detectors that rely solely on the temporal summation of excitation. The results suggest that, in addition to high Kv and HCN conductances at rest, the addition of dendritic inhibition transforms the magnitude and timing of SGN signals as they arrive in the cell body, which may expand the response selectivity of an octopus cell and allow them to become a slightly leakier integrator that can accumulate evidence beyond onsets. Although, this inhibition is difficult to detect because of shunting, our data demonstrate that it is both present and impactful.

As well as needing to work beyond onsets, an effective coincidence detector in the auditory system must also function reliably across a range of sound intensities. Intensity information is encoded by the number and types of SGNs that are activated in the cochlea. The Ia, Ib, and Ic molecular subtypes defined in mouse[50,51,53] broadly correspond to the anatomically and physiologically defined subtypes described across species[52,74]. We find that the majority of inputs onto octopus cells come from Ia SGNs, which most closely correspond to the low-threshold, highspontaneous rate population. Consistent with this result, single-unit SGN recordings in cats demonstrated a bias towards low-threshold, high-spontaneous rate axon collaterals in the octopus cell area[44]. Low-threshold SGNs are also characterized by short first spike latencies and low temporal jitter[75–78]. A hallmark of the octopus cell is the fact that it only fires action potentials when many SGN inputs are activated within a narrow period of time[79]. The presence of many low-threshold and temporally precise inputs on the octopus cell may help ensure that coincidence detection still works reliably for quiet sounds. Further, Ia inputs onto octopus cells do not exhibit pairedpulse depression, similar to low levels of depression seen in Ia inputs to bushy cells[80]. The presence of SGN inputs without paired-pulse depression could be beneficial for encoding sustained auditory signals. Finally, while Ia SGNs are over-represented, Ib and Ic inputs are also present. Since precise, low-threshold SGN responses can be saturated by background noise such that responses to relevant stimuli are masked[10,75,78,81], recruitment of higher threshold SGNs at higher sound intensities may compensate for this tradeoff.

The presence of inhibitory inputs onto dendrites is a fundamental feature of the nervous system and, in other systems, contributes to a neuron's final computation. For example, direction selectivity computations in dendrites of retinal cells require excitation-inhibition interactions in dendritic compartments[82,83]. In pyramidal cells of the cortex and hippocampus, the spatial distribution of inhibition impacts dendritic non-linearities in a branch-selective manner[73,84–88]. However, octopus cells do not share all mechanisms for dendritic computation seen in cortical and hippocampal neurons. Resting conductances and low-threshold potassium conductances may suppress voltage-gated calcium spikes and attenuate the magnitude of action potentials as they backpropagate through the soma and dendritic tree[21,89–91]. Therefore, subthreshold dendritic integration of coincident excitation and local inhibition may be the primary computation that occurs in octopus cell dendrites before action potential generation near the soma.

Although this work uncovers a role for inhibition, a deeper understanding of octopus cell computations will require determining what information is carried by inhibitory inputs. Despite the well-established presence of presynaptic glycinergic puncta in the octopus cell area[92–95] and glycinergic receptor expression in octopus cells[96–100], it is unknown where glycinergic innervation originates. Local neurons within the CNC could provide inhibition; however it remains unclear whether octopus cells receive connections from D-Stellate[56], L-Stellate[101], or

tuberculoventral cells[102]. Outside of the CNC, terminal degeneration experiments in cats suggested the superior periolivary nucleus (SPON) and the ventral division of the lateral lemniscus (VNLL) as potential sources of descending inhibition to the octopus cell area[103]. Octopus cells provide excitatory input to both the SPON[104–108] and the VNLL[32,109–113], raising the possibility of feedback inhibition from the auditory brainstem as a circuit mechanism that elongates temporal summation windows during ongoing stimuli. Such descending feedback inhibition is not rapid enough to prevent or alter the characteristic octopus cell onset response, but could change the effective coincidence detection window as the stimulus continues or limit the duration of the response. Future studies will be required to identify the source of inhibition and its organization within dendritic compartments. If inhibitory inputs tonotopically match the local, narrowly-tuned dendritic SGN inputs, it is possible that frequency-matched inhibition could influence spectral selectivity or feature extraction. On the other hand, broadly tuned inhibition could reduce depolarization block or serve as a temporal milestone that signals gaps or offsets. Further characterization of *in vivo* octopus cell responses in complex sound environments may clarify the effect of noise on signal detection and reveal additional features of this cell's contributions to perception of the auditory world.

Acknowledgements

We thank Nace Golding (University of Texas at Austin), Matthew McGinley (Baylor College of Medicine), Philip Joris (KU Leuven), and Bernardo Sabatini (Harvard Medical School) for helpful discussions and feedback. Sadie Quinn, Lucy Lee, and Ryan Merrow provided valuable technical assistance. Bruce Bean (Harvard Medical School) generously provided access to electrophysiological equipment. *Slc6a5*$^{tm1.1(Cre)Ksak}$, *Ntng1*$^{em1(Cre)Kfra}$, and *Myo15a*$^{tm1.1(Cre)Ugds}$mice were kindly provided by Wade Regehr (Harvard Medical School), Fan Wang (Massachusetts Institute of Technology), and Stefan Heller (Stanford). We thank Rigoberto Ramirez, Tenzin Paljorwa, and Edgar Ramirez for animal care support. We are grateful to the Neurobiology Imaging Facility (NIF) for software availability and to the HMS Research Instrumentation Core for the design and fabrication of temperature regulation equipment. This work was supported by grants from the BRAIN Initiative 1R01NS118402 to L.V.G., the National Institute on Deafness and Other Communication Disorders 5R01DC009223 to L.V.G. and 1F32DC020070 to L.J.K, the William Randolph Hearst Fund to L.J.K, and the Broad Institute's Stanley Center for Psychiatric Research to S.H. and G.F.

Additional information

Author contributions

Conceptualization, L.J.K. and L.V.G.; Methodology, S.H.; Formal Analysis, L.J.K and S.H.; Investigation, L.J.K, S.M., and S.S.; Resources, G.F.; Writing, L.J.K. and L.V.G.; Visualization, L.J.K. and S.H.; Supervision, G.F. and L.V.G.; Funding Acquisition, L.J.K, G.F., and L.V.G. Declaration of Interests

Declaration of Interests

The authors declare no competing interests.

Materials and Methods

Animal Use and Transgenic Mouse Lines

All procedures were approved by and conducted in accordance with Harvard Medical School Institutional Animal Care and Use Committee. Male and female mice (*Mus musculus*) were bred on a C57BL/6 background at the Harvard Center for Comparative Medicine or obtained from Jackson Laboratories. Mice were housed in groups of up to five animals and maintained on a 12hr light/dark cycle. Transgenic alleles were heterozygous for each transgene for all experimental animals. Descriptions of allele combinations for all experiments can be found in **Supp. Table 1**.

Spiral ganglion neurons (SGNs) and their central axons, i.e. auditory nerve fibers, were targeted using either *Foxg1*$^{\text{tm1.1(Cre)Ddmo}}$ (*Foxg1*$^{\text{Cre}}$)[114] or *Foxg1*$^{\text{Flp}}$, both of which drive robust reporter expression in neurons in the auditory and vestibular ganglion[115,116] and the neocortex[117,118], but not in brainstem or midbrain neurons. *Foxg1*$^{\text{Flp}}$ mice were generated by crossing the *Foxg1*$^{\text{tm1.1Fsh}}$ mouse line[119] with the Tg(EIIa-Cre)C5379Lmgd mouse line[120], then backcrossing to isolate the Flp transgene and remove the Cre transgene.

Inhibitory inputs to octopus cells were targeted with *Slc6a5*$^{\text{tm1.1(Cre)Ksak}}$ mice (*Glyt2*$^{\text{Cre}}$)[121].

Octopus cells were sparsely labeled with the Tg(Thy1-YFP)HJrs (*Thy1*) mouse line[122]. This line labels ~0-15 octopus cells amongst other neurons throughout the brain.

Ib/c SGNs were targeted using the *Ntng1*$^{\text{em1(Cre)Kfra}}$ (*Ntng1*$^{\text{Cre}}$) mouse line, which drives expression in neurons throughout the nervous system (**Supp. Fig. 1F**) and disrupts expression of the endogenous allele[54]. Auditory brainstem responses in adult *Ntng1*$^{\text{Cre/+}}$ mice are normal. Ic SGNs were sparsely targeted with the *Myo15a*$^{\text{tm1.1(Cre)Ugds}}$ (*Myo15*$^{\text{iCre}}$) mouse line[123].

Fluorescent reporters included *Gt(ROSA)26Sor*$^{\text{tm14(CAG-tdTomato)}}$ (Ai14, tdT)[124], *Gt(Rosa)26Sor*$^{\text{tm34.1(CAG-Syp/tdTomato)}}$ (Ai34, syp/tdT), and *Gt(Rosa)26Sor*$^{\text{tm1.2(CAG-EGFP)Fsh}}$ (RCE:FRT, EYFP)[125]. We also used *Gt(Rosa)26Sor*$^{\text{tm32(CAG-COP4*H134R.EYFP)}}$ (Ai32, ChR2)[126] to drive synaptic activity in *in vitro* slice experiments.

Histology and Reconstructions

For immunohistochemical labeling, mice were deeply anesthetized with isoflurane and transcardially perfused with 15mL of 4% paraformaldehyde (PFA) in 0.1M phosphate-buffered saline (PBS) using a peristaltic pump (Gilson). Whole skulls containing brain and cochlea were immediately transferred to 20mL of 4% PFA and post-fixed overnight at 4°C. Fixed brains and cochlea were removed from the skulls and washed with 0.1M PBS.

Brains were collected from mice of both sexes, aged 28-38 days, and embedded in gelatin-albumin hardened with 5% glutaraldehyde and 37% PFA[127]. Sections were cut at 35, 65, or 100μm with a vibrating microtome (Leica VT1000S) and free-floating tissue was collected in 0.1M PBS. For sections less than 65μm, tissue was permeabilized and nonspecific staining was blocked in a solution of 0.2% Triton X-100 and 5% normal donkey serum (NDS, RRID: AB_2337258) in 0.1M PBS for 1 hour. After blocking, tissue was treated with primary antibody in a solution containing 0.2% Triton X-100 and 5% NDS in PBS for 1-2 nights at room temperature. Primary antibodies used were: chicken anti-GFP (1:1000, RRID:AB_10000240), rabbit anti-RFP (1:1000, RRID:AB_2209751), goat anti-calretinin (1:1000, RRID:AB_1000034), and guinea pig anti-VGLUT1 (1:500, RRID:AB_887878). Sections were washed in 0.1M PBS then incubated in a secondary antibody solution (1:1000) containing 0.2% Triton X-100 and 5% NDS for 2-3hrs at room temperature. Tissue sections were mounted on charged slides and coverslipped (Vectashield Hardset Antifade Mounting Medium with DAPI), and imaged using a Zeiss Observer.Z1 confocal microscope.

For 100µm sections, tissue was washed in CUBIC-1A solution[128] for 1hr for strong permeabilization and delipidization[128,129]. Tissue was then further permeabilized and nonspecific staining was blocked in a solution of 0.2% Triton X-100 and 5% NDS in 0.1M PBS for 1hr. After blocking, tissue was treated with primary antibody in a solution containing 0.2% Triton X-100 and 5% NDS in PBS for 4 nights at 37°C. Primary antibodies used were: chicken anti-GFP (1:1000, RRID:AB_10000240), and rabbit anti-RFP (1:1000, RRID:AB_2209751). Sections were then incubated in a secondary antibody solution (1:400) containing 0.2% Triton X-100 and 5% NDS for 4 nights at 37°C. Tissue sections were pre-incubated in CUBIC2 solution, then temporarily mounted on uncharged slides with CUBIC2 solution for immediate imaging using a Zeiss Observer.Z1 confocal microscope.

Octopus cells and synaptic puncta were reconstructed in Imaris (Oxford Instruments). YFP signal from the target octopus cell was used to generate a surface reconstruction and mask syp/tdT signal. Dendrites were reconstructed using the masked YFP signal and separated into 10µm increments. Masked syp/tdT puncta were marked and localized to a 10µm increment of the dendritic tree. Synapse counts, dendrite metrics, and masked channels were exported to Excel (Microsoft) for further analysis.

Cochlea were collected from mice of both sexes, aged 28-42 days. The bony labyrinth of the inner ear was decalcified in 0.5M ethylenediamine tetraacetic acid (EDTA) for 3 nights at 4°C and embedded in gelatin-albumin hardened with 5% glutaraldehyde and 37% PFA. Sections were cut at 65µm with a vibrating microtome (Leica VT1000S) and freefloating tissue was collected in 0.1M PBS. Sections were washed in CUBIC-1A solution for 1hr for strong permeabilization and delipidization. Tissue was further permeabilized and nonspecific staining was blocked in a solution of 0.2% Triton X-100 and 5% NDS in 0.1M PBS for 1hr. After blocking, tissue was treated with primary antibody in a solution containing 0.2% Triton X-100 and 5% NDS in PBS for 2 nights at room temperature. Primary antibodies used were: chicken anti-GFP (1:1000, RRID:AB_10000240), rabbit anti-RFP (1:1000, RRID:AB_2209751), goat anti-calretinin (1:1000, RRID:AB_1000034). Sections were then incubated in a secondary antibody solution (1:500) containing 0.2% Triton X-100 and 5% normal goat serum for 2-3hrs at room temperature. Tissue sections were mounted on charged slides, coverslipped (Vectashield Hardset Antifade Mounting Medium with DAPI), and imaged using a Zeiss Observer.Z1 confocal microscope.

Acute Slice Electrophysiology

Data were obtained from mice of both sexes, aged 24-47 days. Mice were deeply anesthetized with isoflurane and perfused transcardially with 3mL of 35°C artificial cerebral spinal fluid (ACSF; 125mM NaCl, 25mM glucose, 25mM $NaHCO_3$, 2.5mM KCl, 1.25mM NaH_2PO_4, 1.4Mm $CaCl_2$, and 1.6mM $MgSO_4$, pH adjusted to 7.45 with NaOH). For high calcium concentration experiments presented in **Fig. 3C**, ACSF contained 125mM NaCl, 25mM glucose, 25mM $NaHCO_3$, 2.5mM KCl, 1.25mM NaH_2PO_4, 2.4mM $CaCl_2$, and 1.3mM $MgSO_4$. Mice were rapidly decapitated and the brain was removed and immediately submerged in ACSF. Brains were bisected and 250µm slices were prepared in the sagittal plane with a vibrating microtome (Leica VT1200S; Leica Systems). Prepared slices were incubated for 30min at 35°C, then allowed to recover at room temperature for at least 30min. ACSF was continuously bubbled with 95% O_2/5% CO_2.

Whole-cell recordings were conducted at 35°C using a Multiclamp 700B (Molecular Devices) in current-clamp mode with experimenter adjusted and maintained bridge balance and capacitance compensation. Data were filtered at 12kHz, digitized at 83–100kHz, and acquired using pClamp9 (Molecular Devices). Neurons were visualized using infrared Dodt gradient contrast (Zeiss Examiner.D1; Zeiss Axiocam 305 mono). Glass recording electrodes (3–7MΩ) were wrapped in parafilm to reduce capacitance and filled with an intracellular solution containing 115mM Kgluconate, 4.42mM KCl, 0.5mM EGTA, 10mM HEPES, 10mM Na_2Phosphocreatine, 4mM MgATP, 0.3mM NaGTP, and 0.1% biocytin, osmolality adjusted to 300mmol/kg with sucrose, pH adjusted to 7.30 with KOH. All membrane potentials are corrected for a -11mV junction potential.

For optogenetic activation, full-field 475nm blue light was presented through a 20x immersion objective (Zeiss Examiner.D1). Onset, duration, and intensity of light was controlled by a Colibri5 LED Light Source (Zeiss). Light intensity at the focal plane ranged between 1.9 and 4.1mW/mm^2, corresponding to 6% and 10% intensity on the Colibri5 system. For electrical stimulation, glass stimulating electrodes were placed in the auditory nerve root and 20µs current pulses were generated with a DS3 current stimulator (Digitimer). Light or electrical stimulation intensity was adjusted during the experiment to evoke subthreshold EPSPs, not spikes. During analysis, EPSPs and spikes were distinguished by screening all events with a phase plot analysis. Only stimulation events that evoked EPSPs unambiguously were included for analysis. When presenting electrical and light stimulation together, a series of stimulation pairings with shuffled onset timings was presented to account for cell to cell variability in EPSP and IPSP timings. Data presented is for the stimulation pairings that evoked a maximal shift in EPSP timings.

Analysis and Statistical Tests

Cell counts and habenula measurements were performed in ImageJ/FIJI software (National Institutes of Health). Electrophysiology data were analyzed using custom scripts and NeuroMatic analysis routines[130] in Igor Pro (Wavemetrics).

For data with equal variance (Levene's test), one-way ANOVAs with Tukey's HSD post hoc test were used where appropriate to determine statistical significance. For data with non-homogenous variances, oneway ANOVAs with a Welch F test were used with a Tukey's HSD post hoc test. Errors and error bars report standard deviation (SD) or standard error of the mean (SEM) as noted in figure legends and throughout the text.

Computational Modelling

Computer simulations were performed using the NEURON 8.2 simulation environment[131], with an integration time constant of 25µs. The morphology of the octopus neuron was obtained from McGinley et al., 2012[30]. The active and passive properties of the model were optimized to match the experimental recordings. We set the passive parameters as follows: internal or axial resistance (R_i or R_a) to 150Ω.cm, membrane resistance (R_m) to 5KΩ.cm^2, capacitance (C_m) to 0.9µF/Cm^2 and resting membrane potential (V_m) to -65mV. Ion-channel kinetics, maximum conductance densities, Q10 (3), and temperature (22°C) were obtained from and matched to Manis and Campagnola, 2018[71] and the maximal conductances were adjusted using a scaling factor (scl) to align qualitatively with experimental data (**Supp. Fig. 4A-B**): fast Na^+ ($\bar{g}_{Na} = 0.83$), fast transient K^+ ($\bar{g}_{KA} = 0.07$), high threshold K^+ ($\bar{g}_{KHT} = 0.1875$), low-voltage activated K^+ ($\bar{g}_{KLT} = 0.75$), hyperpolarization-activated cyclic nucleotide-gated (HCN; $\bar{g}_h = 0.07$) and leak K^+ ($\bar{g}_{leak} = 0.0017$). All conductances were uniformly distributed across dendrites and soma, except for HCN conductance, which was only present in dendrites. A baseline scaling factor of 1 was applied under control conditions and 0 under Kv+HCN block conditions. AMPA conductance (G_{AMPA}) was set to 5nS to align with experimental data (**Fig. 5F**), and glycine conductance (G_{Gly}) was set to 1nS to match experimental observations (**Fig. 4E**). Reversal potentials for HCN, Na^+, and K^+ respectively were (in mV), E_h= -38, E_{Na}= 50 and E_K= -70. Excitatory AMPA synaptic conductance and inhibitory glycine synaptic conductance were introduced in the proximal and distal dendrites to test the impact of dendritic inhibition on the EPSP height and peak time. The magnitudes of synaptic conductances were tuned to fall within the range seen during experimental data collection. The rise and decay time of AMPA and glycine conductances were tuned to 0.3ms and 3ms respectively, to match experimental data. The reversal potential of AMPA and glycine conductance was set to 0mV and -80mV respectively.

	Experimental Genotype	*Abbreviation*	*Description*
Fig. 1B	*Glyt2*$^{Cre/+}$; Ai34$^{tg/+}$	*Glyt2*-syp/tdT	syp/tdT in *Glyt2* inhibitory neurons
Fig. 1C	*Glyt2*$^{Cre/+}$; Ai34$^{tg/+}$; *Thy1*$^{tg/+}$	*Glyt2*-syp/tdT; *Thy1*	syp/tdT in *Glyt2* inhibitory neurons; YFP octopus cells
Fig. 1D; 1F-G, black	*Foxg1*$^{Cre/+}$; Ai34$^{tg/+}$; *Thy1*$^{tg/+}$	*Foxg1*-syp/tdT; *Thy1*	syp/tdT in *Foxg1* SGNs; YFP octopus cells
Fig. 1E; 1F-G, green	*Glyt2*$^{Cre/+}$; Ai34$^{tg/+}$; *Thy1*$^{tg/+}$	*Glyt2*-syp/tdT; *Thy1*	syp/tdT in *Glyt2* inhibitory neurons; YFP octopus cells
Fig. 2B	*Ntng1*$^{Cre/+}$; Ai14$^{tg/+}$; *Foxg1*$^{Flp/+}$; RCE:FRT$^{tg/+}$	*Ntng1*-tdT; *Foxg1*-EYFP	tdT in *Ntng1* Ib/c SGNs; EYFP in all SGNs
Fig. 2C-F	*Ntng1*$^{Cre/+}$; Ai34$^{tg/+}$; *Thy1*$^{tg/+}$	*Ntng1*-syp/tdT; *Thy1*	syp/tdT in *Ntng1* Ib/c SGNs; YFP octopus cells
Fig. 3A-C, black	*Foxg1*$^{Cre/+}$; Ai32$^{tg/+}$	*Foxg1*-ChR2	ChR2 in *Foxg1* SGNs
Fig. 3A-C, magenta	*Ntng1*$^{Cre/+}$; Ai32$^{tg/+}$	*Ntng1*-ChR2	ChR2 in *Ntng1* Ib/c SGNs
Fig. 4A-C	*Glyt2*$^{Cre/+}$; Ai32$^{tg/+}$	*Glyt2*-ChR2	ChR2 in *Glyt2* inhibitory neurons
Fig. 5F-H	*Glyt2*$^{Cre/+}$; Ai32$^{tg/+}$	*Glyt2*-ChR2	ChR2 in *Glyt2* inhibitory neurons
Fig. S1A-C	*Ntng1*$^{Cre/+}$; Ai14$^{tg/+}$; *Foxg1*$^{Flp/+}$; RCE:FRT$^{tg/+}$	*Ntng1*-tdT; *Foxg1*-EYFP	tdT in *Ntng1* Ib/c SGNs; EYFP in all SGNs
Fig. S1D-E	*Ntng1*$^{Cre/+}$; Ai14$^{tg/+}$	*Ntng1*-tdT	tdT in *Ntng1* Ib/c SGNs and other neurons
Fig. S1F	*Ntng1*$^{Cre/+}$; Ai34$^{tg/+}$	*Ntng1*-syp/tdT	syp/tdT in *Ntng1* Ib/c SGNs
Fig. S2A-F	*Myo15*$^{iCre/+}$; Ai14$^{tg/+}$; *Foxg1*$^{Flp/+}$; RCE:FRT$^{tg/+}$	*Myo15*-tdT; *Foxg1*-EYFP	tdT in *Myo15* Ic SGNs; EYFP in all SGNs
Fig. S2G-I	*Myo15*$^{iCre/+}$; Ai34$^{tg/+}$; *Thy1*$^{tg/+}$	*Myo15*-syp/tdT; *Thy1*	syp/tdT in *Myo15* Ic SGNs; YFP octopus cells

Supplementary Table 1.

Summary and description of experimental genotypes presented in figures.

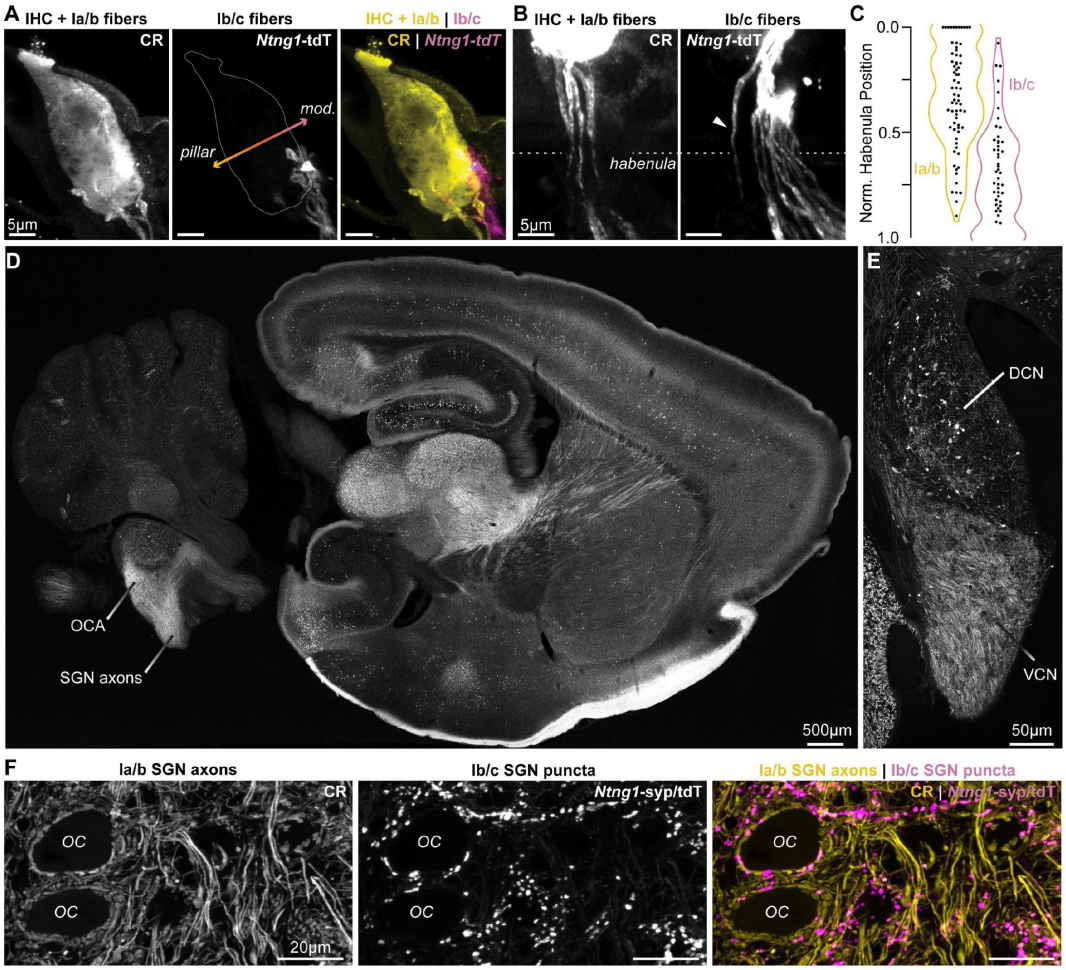

Supplementary Figure 1.

Ntng1^{Cre} has high specificity for Ib/c SGNs.

(A) Calretinin immunopositive (CR+) Ia/b spiral ganglion neuron (SGN) peripheral fibers (CR, yellow) preferentially innervate the pillar side of inner hair cells (IHCs). Ib/c SGN peripheral fibers with *Ntng1*^{Cre}-mediated expression of tdTomato (*Ntng1*-tdT, magenta) preferentially innervate the modiolar side of IHCs. IHCs also immunolabel for CR. **(B)** CR+ Ia/b SGN fibers (yellow) pass through the pillar side of the habenula while *Ntng1*-tdT+ Ib/c SGN fibers (magenta) pass through the modiolar side. Arrowhead highlights a *Ntng1*-tdT fiber passing through the pillar side of the habenula but ultimately terminating on the modiolar side of the IHC. **(C)** Normalized position of CR+ Ia/b (yellow) and *Ntng1*-tdT+ Ib/c (magenta) fibers in the habenula (*n* = 124 fibers; 5 mice). **(D)** In the central nervous system, *Ntng1*-tdT is present throughout the brain, but is restricted to SGN axons in the ventral cochlear nucleus where the octopus cell area (OCA) is found. **(E)** A coronal section of the cochlear nucleus highlights *Ntng1*-tdT SGN axons in the ventral cochlear nucleus (VCN) and scattered *Ntng1*-tdT somas in the dorsal cochlear nucleus (DCN). **(F)** In the octopus cell area, CR immunolabel is present in Ia/b SGN axons and puncta. As in the ganglion, CR co-labels with some Ib/c puncta (*Ntng1*-syp/tdT).

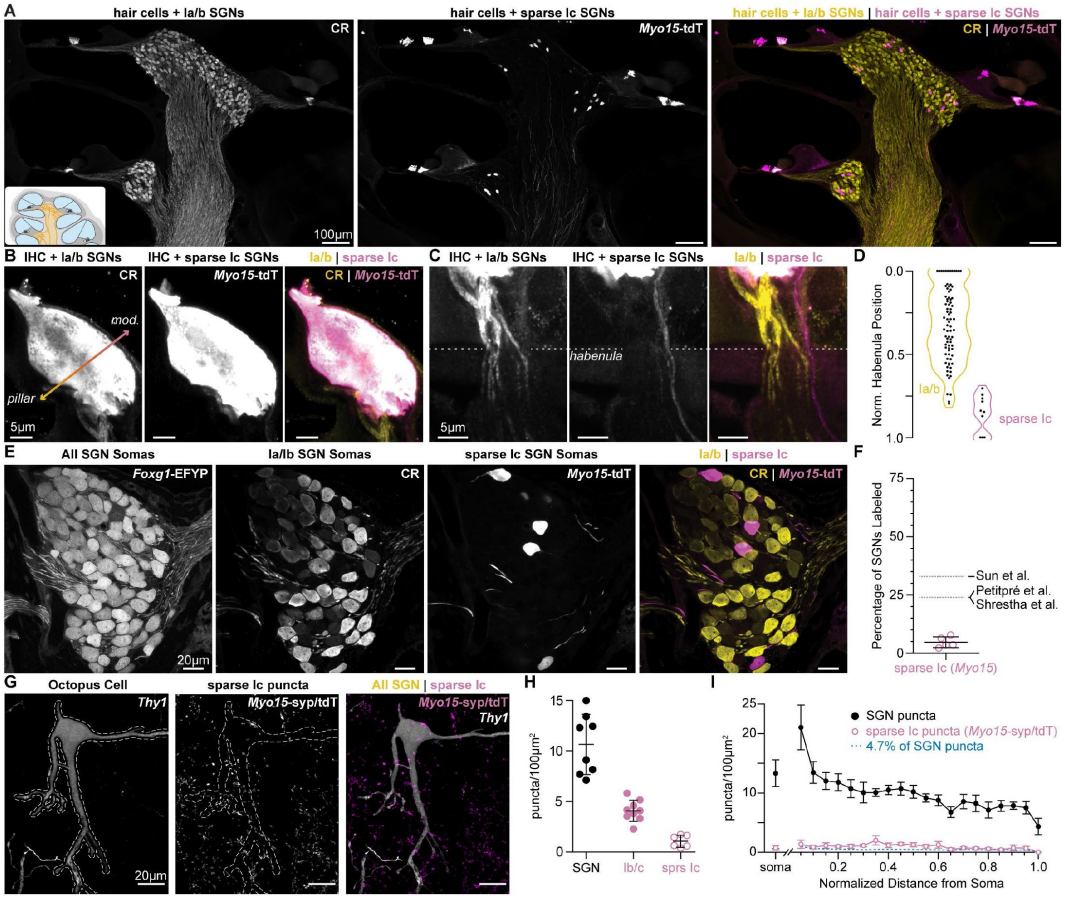

Supplementary Figure 2.

Myo15^{iCre} sparsely labels Ic SGNs.

(A) Cochlear sections with calretinin (CR) immunolabeling of hair cells and type Ia/b spiral ganglion neurons (SGNs) and *Myo15*^{iCre}-mediated expression of tdTomato (*Myo15*-tdT) in hair cells and some type Ic SGNs. **(B)** CR+ Ia/b SGN fibers (yellow) preferentially innervate the pillar side of inner hair cells (IHCs). Sparse Ic SGN fibers with *Myo15*-tdT (magenta) preferentially innervate the modiolar side of IHCs. IHCs label with both tdT and CR. **(C)** CR+ Ia/b SGN fibers (yellow) pass through the pillar side of the habenula while sparsely labeled *Myo15*-tdT+ Ic SGN fibers (magenta) pass through the modiolar side. **(D)** Normalized position of CR+ Ia/b (yellow) and *Myo15*-tdT+ Ic (magenta) SGN fibers along the pillar to modiolar axis of the habenula (*n* = 90 fibers; 4 mice). **(E)** 65µm cochlear section containing SGN somas. SGNs have variable levels of calretinin (CR) immunolabeling corresponding to the three molecular subtypes. Ia/b SGN somas label with high and medium levels of CR, respectively. Ic somas label with very low levels of CR. *Myo15*-tdT is sparsely found in Ic SGNs. All SGN somas are labeled with *Foxg1*^{Flp}-mediated expression of EYFP (*Foxg1*-EYFP). **(F)** tdT+CRSGNs make up 4.7 ± 2.3% of the SGN population (*n* = 2150 neurons, 5 mice), indicating sparse reporter expression. Data are presented as mean ± SD; individual data points signify percent coverage per animal. Dotted lines are estimated percentages for type Ic SGNs from 1: Petitpré et al., 2018, 2: Shrestha et al., 2018, and 3: Sun et al., 2018. **(G)** A sparsely labeled *Thy1* octopus cell has few *Myo15*-syp/tdT puncta near its soma and dendrites. **(H)** Density of all SGN (black: data from **Fig. 1D**), Ib/c SGN (magenta: data from **Fig. 2D**), and sparse Ic SGN inputs (open magenta circles: 1.1 ± 0.6, *n* = 6 cells, 3 mice). Data are presented as mean ± SD. Markers represent the total puncta density computed per reconstructed octopus cell. **(I)** Puncta density per 100µm^2 of soma surface area (all SGN, black: data from **Fig. 1E**; sparse I/c inputs, magenta open circles: 0.7 ± 0.4, *n* = 6 cells, 3 mice) and density along the length of the dendritic tree, relative to the soma. Data are presented as mean ± SEM.

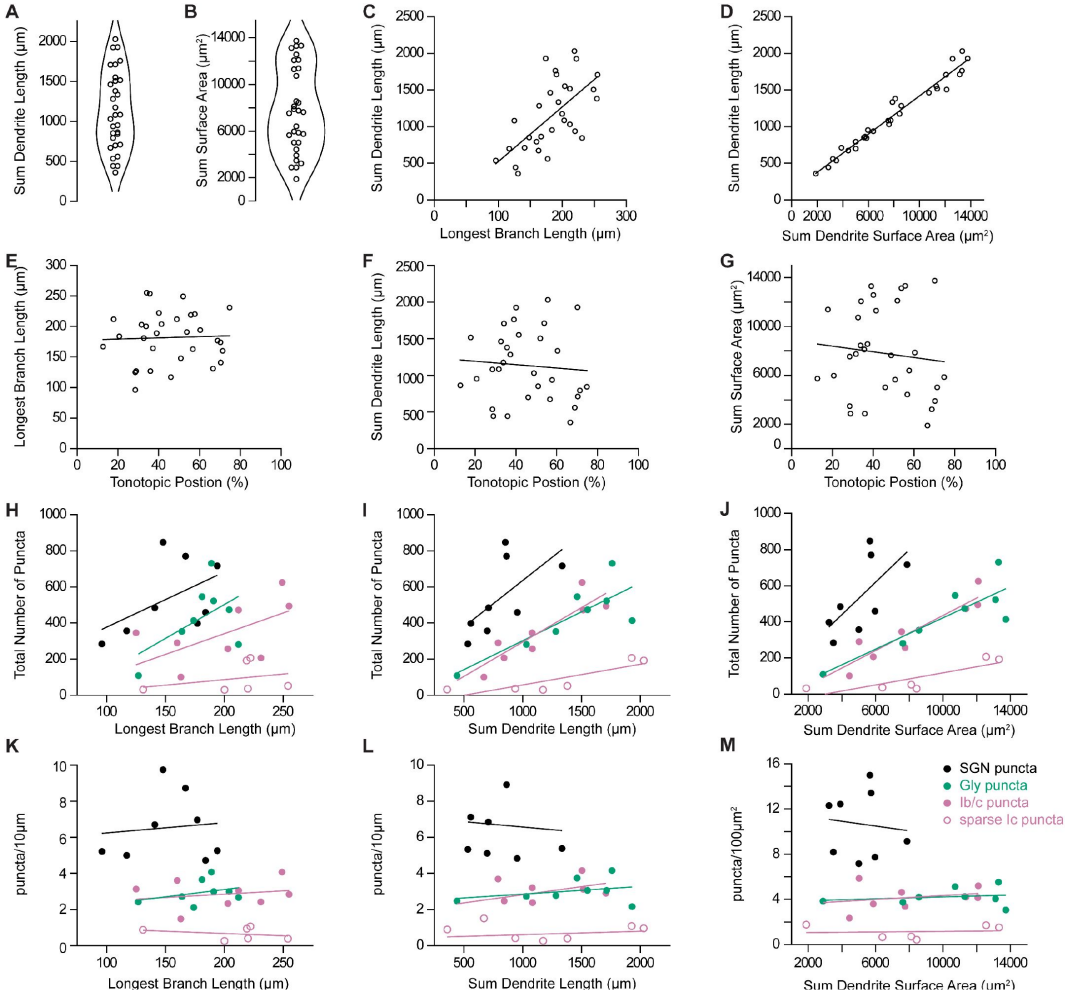

Supplementary Figure 3.

Dendritic and synaptic reconstructions of octopus cells.

(A) Total length of reconstructed dendritic arbors for 31 octopus cells. **(B)** Total surface area of reconstructed dendritic arbors for 31 octopus cells. **(C)** Octopus cell reconstructions were normalized to the longest reconstructed dendrite. Total length of reconstructed dendrites correlated with the longest branch per neuron. **(D)** Total length of reconstructed dendrites correlated with total dendritic surface area. **(E-G)** Longest branch length, total dendrite length, and total surface area compared to estimated position of the octopus cell soma in the tonotopic organization of the octopus cell area. **(H-J)** Total number of reconstructed spiral ganglion neuron (SGN) puncta (*Foxg1*-syp/tdT, black), inhibitory puncta (*Glyt2*-syp/tdT, green), Ib/c SGN puncta (*Ntng1*-syp/tdT, magenta), and sparse Ic SGN puncta (*Myo15*-syp/tdT, open magenta circles) compared to the longest branch length, total dendrite length, and total dendrite surface area. **(K-M)** Density of reconstructed SGN puncta (*Foxg1*-syp/tdT, black), inhibitory puncta (*Glyt2*-syp/tdT, green), Ib/c SGN puncta (*Ntng1*-syp/tdT, magenta), and sparse Ic SGN puncta (*Myo15*-syp/tdT, open magenta circles) compared to longest branch length, total dendrite length, and total dendrite surface area.

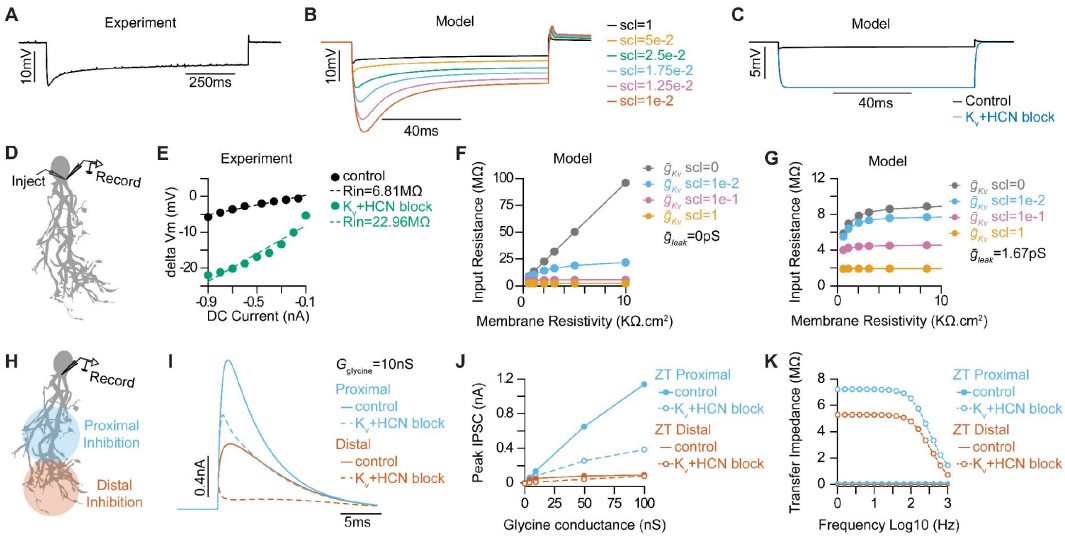

Supplementary Figure 4.

Optimizing active and passive properties of an octopus cell model.

(A) Subthreshold somatic voltage response to a -800pA hyperpolarizing current injection in an *in vitro* whole-cell current clamp recording of an octopus cell. **(B)** Somatic voltage responses from a morphologically realistic octopus cell model to a -800pA current injection for various scaling factors (scl) of maximal conductances of $\bar{g}_{KLT}$, $\bar{g}_{KHT}$, $\bar{g}_{KA}$ and $\bar{g}_{h}$.**(C)** Comparison of somatic hyperpolarizations to a -800pA current injection in the model reproducing experimental data during control (black) and Kv and HCN block conditions (blue). **(D)** Illustration of injection and recording locations for panels *E-G* in a morphologically realistic octopus cell model. **(E)** Current-voltage (IV) relationships from a representative experimental octopus cell recorded in control ACSF and with Kv and HCN block. Dotted lines plot linear fits of the experimental data. The slope of the dotted line estimates Rin. **(F-G)** Impact of leak conductance $(\bar{g}_{leak})$ and scaling factor (scl) on passive properties of the model with $\bar{g}_{leak}$=0pS *(F)* and $\bar{g}_{leak}$=1.67pS *(G)* for various scaling factor values (indicated in different colors). **(H)** Illustration of injection and recording locations for panels *I-K* in a morphologically realistic octopus cell model. **(I)** Somatically recorded inhibitory post synaptic currents (IPSCs) recorded from glycinergic synapses in proximal (blue) and distal (orange) stimulation during control (solid) and Kv and HCN block conditions (dotted). **(J)** Peak IPSC magnitude as function of glycine conductance in proximal (blue) and distal (orange) stimulation during control (solid) and Kv and HCN block conditions (dotted). **(K)** Transfer impedance as function of frequency from proximal dendrites to soma (blue) and distal dendrites to soma (orange) during control (solid) and Kv and HCN block conditions (dotted).

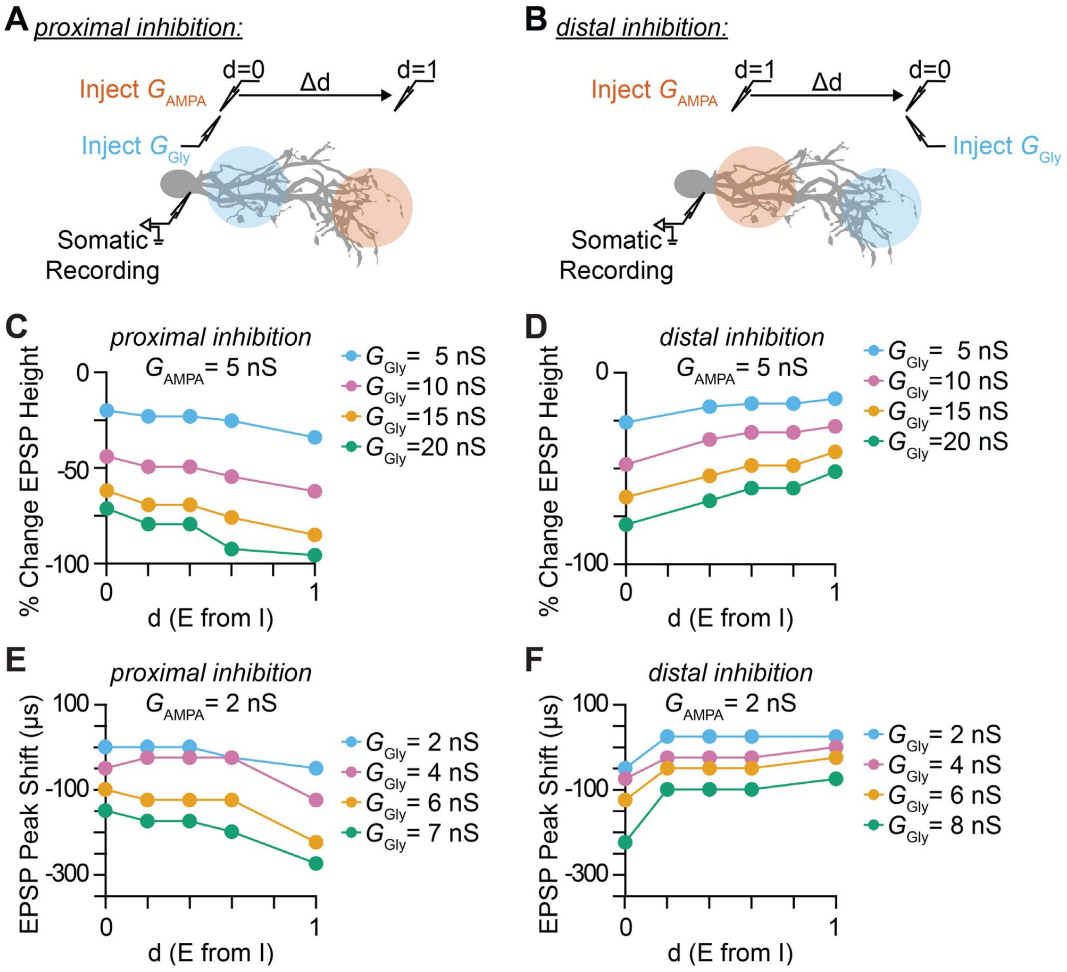

Supplementary Figure 5.

Impact of inhibitory synaptic location and distance between excitatory and inhibitory synapse on somatic EPSP amplitude and timing.

(A-B) Illustration of injection and recording locations for proximal *(A)* and distal *(B)* inhibition paradigms and the normalized relative distance (d) between excitatory synapses. The impact that the location of dendritic inhibition has on somatic EPSPs is primarily determined by the local potential change by an EPSP and the attenuation or the length constant (λ) of the IPSP towards the excitatory synaptic location. The exponential decay of membrane voltage is asymmetric, with lower λ for the open end and higher λ for sealed end propagation. Distal parts of the dendrites have higher local input resistance and lower attenuation of IPSP due to the sealed end. **(C-D)** Percentage change in somatic EPSP height with dendritic glycinergic inhibition as function of normalized distance between excitatory and inhibitory synapses in proximal *(C)* and distal *(D)* inhibition for various E/I ratio with excitatory AMPA conductance (G_{AMPA}) set at 5nS. Average shown in black with SEM in shaded region. **(E-F)** Somatic EPSP peak time shift with dendritic glycinergic inhibition as function of normalized distance between excitatory and inhibitory synapses in proximal *(E)* and distal *(F)* inhibition for various E/I ratio with excitatory AMPA conductance (G_{AMPA}) set at 2nS. Average shown in black with SEM in shaded region.

References

1. Shamma S.A., Elhilali M., Micheyl C. (2011) **Temporal co-herence and attention in auditory scene analysis** *Trends Neurosci* **34**:114–123 https://doi.org/10.1016/j.tins.2010.11.002

2. Pressnitzer D., Suied C., Shamma S. (2011) **Auditory scene analysis: The sweet music of ambiguity** *Front. Hum. Neurosci* **5**

3. De No R.L. (1933) **The central projection of the nerve endings of the internal ear** *The Laryngoscope* **43**:1–38 https://doi.org/10.1288/00005537-193301000-00001

4. Fekete D.M., Rouiller E.M., Liberman M.C., Ryugo D.K. (1984) **The Central Projections of Intracellularly Labeled Auditory Nerve Fibers in Cats** *J. Comp. Neurol* :432–450

5. Liberman M.C. (1991) **Central projections of auditory-nerve fibers of differing spontaneous rate. I. Anteroventral cochlear nucleus** *J. Comp. Neurol* **313**:240–258 https://doi.org/10.1002/cne.903130205

6. Brown M.C., Ledwith J.V. (1990) **Projections of thin (type-II) and thick (type-I) auditory-nerve fibers into the cochlear nucleus of the mouse** *Hear. Res* **49**:105–118 https://doi.org/10.1016/0378-5955(90)90098-A

7. Leake P.A., Snyder R.L. (1989) **Topographic organization of the central projections of the spiral ganglion in cats** *J. Comp. Neu-rol* **281**:612–629 https://doi.org/10.1002/cne.902810410

8. Sachs M.B., Abbas P.J. (1974) **Rate versus level functions for auditory-nerve fibers in cats: tone-burst stimuli** *J. Acoust. Soc. Am* **56**:1835–1847 https://doi.org/10.1121/1.1903521

9. Liberman M.C. (1982) **Single-Neuron Labeling in the Cat Auditory Nerve** *Science* **216**:1239–1241

10. Liberman M.C. (1978) **Auditory-nerve response from cats raised in a low-noise chamber** *J. Acoust. Soc. Am* **63**:442–455 https://doi.org/10.1121/1.381736

11. Evans E.F., Palmer A.R. (1980) **Relationship between the dynamic range of cochlear nerve fibres and their spontaneous activity** *Exp. Brain Res* **40**:115–118 https://doi.org/10.1007/BF00236671

12. Taberner A.M., Liberman M.C. (2005) **Response properties of single auditory nerve fibers in the mouse** *J. Neurophysiol* **93**:557–569 https://doi.org/10.1152/jn.00574.2004

13. Palmer A.R., Evans E.F. (1980) **Cochlear fibre rate-intensity functions: No evidence for basilar membrane nonlinearities** *Hear. Res* **2**:319–326 https://doi.org/10.1016/0378-5955(80)90065-9

14. Winter I.M., Robertson D., Yates G.K. (1990) **Diversity of characteristic frequency rate-intensity functions in guinea pig auditory nerve fibres** *Hear. Res* **45**:191–202 https://doi.org/10.1016/0378-5955(90)90120-E

15. Osen K.K. (1969) **The intrinsic organization of the cochlear nuclei in the cat** *Acta Otolaryngol. (Stockh* **67**:352–359 https://doi.org/10.3109/00016486909125462

16. Osen K.K. (1969) **Cytoarchitecture of the cochlear nuclei in the cat** *J. Comp. Neurol* **136**:453–483 https://doi.org/10.1002/cne.901360407

17. Godfrey D.A., Kiang N.Y.S., Norris B.E. (1975) **Single unit activity in the posteroventral cochlear nucleus of the cat** *J. Comp. Neurol* **162**:247–268 https://doi.org/10.1002/cne.901620206

18. Recio-Spinoso A., Rhode W.S. (2020) **Information Processing by Onset Neurons in the Cat Auditory Brainstem** *JARO - J. Assoc. Res. Otolaryngol* **21**:201–224 https://doi.org/10.1007/s10162-020-00757-0

19. Rhode W.S., Smith P.H., Oertel D. (1983) **Physiological response properties of cells labeled intracellularly with horseradish peroxidase in cat dorsal cochlear nucleus** *J. Comp. Neurol* **213**:426–447 https://doi.org/10.1002/cne.902130407

20. Ritz L.A., Brownell W.E. (1982) **Single unit analysis of the posteroventral cochlear nucleus of the decerebrate cat** *Neuroscience* **7**:1995–2010 https://doi.org/10.1016/0306-4522(82)90013-6

21. Golding N.L., Ferragamo M.J., Oertel D. (1999) **Role of intrinsic conductances underlying responses to transients in octopus cells of the cochlear nucleus** *J. Neurosci* **19**:2897–2905 https://doi.org/10.1523/jneurosci.19-08-02897.1999

22. Bal R., Oertel D. (2000) **Hyperpolarization-activated, mixedcation current (I(h)) in octopus cells of the mammalian cochlear nucleus** *J. Neurophysiol* **84**:806–817 https://doi.org/10.1152/jn.2000.84.2.806

23. Bal R., Oertel D. (2001) **Potassium currents in octopus cells of the mammalian cochlear nucleus** *J. Neurophysiol* **86**:2299–2311 https://doi.org/10.1152/jn.2001.86.5.2299

24. Cao X.J., Oertel D. (2017) **Genetic perturbations suggest a role of the resting potential in regulating the expression of the ion channels of the KCNA and HCN families in octopus cells of the ventral cochlear nucleus** *Hear. Res* **345**:57–68 https://doi.org/10.1016/j.heares.2017.01.001

25. Golding N.L., Robertson D., Oertel D. (1995) **Recordings from slices indicate that octopus cells of the cochlear nucleus detect coincident firing of auditory nerve fibers with temporal precision** *J. Neurosci* **15**:3138–3153 https://doi.org/10.1523/jneuro-sci.15-04-03138.1995

26. Golding N.L., Oertel D. (2012) **Synaptic integration in den-drites: Exceptional need for speed** *J. Physiol* **590**:5563–5569 https://doi.org/10.1113/jphysiol.2012.229328

27. Manis P.B., Marx S.O. (1991) **Outward currents in isolated ventral cochlear nucleus neurons** *J. Neurosci* **11**:2865–2880 https://doi.org/10.1523/jneurosci.11-09-02865.1991

28. Oertel D. (1983) **Synaptic responses and electrical properties of cells in brain slices of the mouse anteroventral cochlear nucleus** *J. Neurosci* **3**:2043–2053 https://doi.org/10.1523/jneurosci.03-10-02043.1983

29. McGinley M.J., Cuntz H., Remme M. W. H., Torben-Nielsen B. (2014) **Rapid Integration Across Tonotopy by Indi-vidual Auditory Brainstem Octopus Cells** *The Computing Dendrite, From Structure to Function* Springer New York :223–243 https://doi.org/10.1007/978-1-4614-8094-5_14

30. McGinley M.J., Liberman M.C., Bal R., Oertel D. (2012) **Generating Synchrony from the Asynchronous: Compensation for Cochlear Traveling Wave Delays by the Dendrites of Individual Brainstem Neurons** *J. Neurosci* **32**:9301–9311 https://doi.org/10.1523/jneurosci.0272-12.2012

31. Lu H.W., Smith P.H., Joris P.X. (2018) **Submillisecond monaural coincidence detection by octopus cells** *Acta Acust. United Acust* **104**:852–855 https://doi.org/10.3813/AAA.919238

32. Smith P.H., Massie A., Joris P.X. (2005) **Acoustic stria: Anatomy of physiologically characterized cells and their axonal projection patterns** *J. Comp. Neurol* **482**:349–371 https://doi.org/10.1002/cne.20407

33. Smith P.H., Joris P.X., Banks M.I., Yin T.C.T., Merchán M. A., Juiz J. M., Godfrey D. A., Mugnaini E. (1993) **Responses of Cochlear Nucleus Cells and Projections of their Axons** *The Mammalian Cochlear Nuclei: Organization and Function NATO ASI series* Springer US :349–360 https://doi.org/10.1007/978-1-4615-2932-3_27

34. Cai Y., McGee J., Walsh E.J. (2000) **Contributions of Ion Conductances to the Onset Responses of Octopus Cells in the Ventral Cochlear Nucleus: Simulation Results** *J. Neurophysiol* **83**:301–314 https://doi.org/10.1152/jn.2000.83.1.301

35. Cai Y., Walsh E.J., McGee J. (1997) **Mechanisms of Onset Responses in Octopus Cells of the Cochlear Nucleus: Implications of a Model** *J. Neurophysiol* **78**:872–883 https://doi.org/10.1152/jn.1997.78.2.872

36. Kipke D.R., Levy K.L. (1997) **Sensitivity of the cochlear nucleus octopus cell to synaptic and membrane properties: A model-ing study** *J. Acoust. Soc. Am* **102**:403–412 https://doi.org/10.1121/1.419762

37. Levy K.L., Kipke D.R. (1998) **Mechanisms of the cochlear nucleus octopus cell's onset response: Synaptic effectiveness and threshold** *J. Acoust. Soc. Am* **103**:1940–1950 https://doi.org/10.1121/1.421346

38. Levy K.L., Kipke D.R. (1997) **A computational model of the cochlear nucleus octopus cell** *J. Acoust. Soc. Am* **102**:391–402 https://doi.org/10.1121/1.419761

39. Rebhan M., Leibold C. (2021) **A phenomenological spiking model for octopus cells in the posterior–ventral cochlear nucleus** *Biol. Cybern* **115**:331–341 https://doi.org/10.1007/s00422-021-00881-x

40. Spencer M., Grayden D., Bruce I., Meffin H., Burkitt A. (2012) **An investigation of dendritic delay in octopus cells of the mammalian cochlear nucleus** *Front. Comput. Neurosci* **6** https://doi.org/10.3389/fncom.2012.00083

41. Lu H.-W., Smith P.H., Joris P.X. (2022) **Mammalian octopus cells are direction selective to frequency sweeps by excitatory syn-aptic sequence detection** *Proc. Natl. Acad. Sci* **119** https://doi.org/10.1073/pnas.2203748119

42. Gómez-Nieto R., Rubio M.E. (2009) **A bushy cell network in the rat ventral cochlear nucleus** *J. Comp. Neurol* **516**:241–263 https://doi.org/10.1002/cne.22139

43. Zhou J., Nannapaneni N., Shore S. (2007) **Vessicular gluta-mate transporters 1 and 2 are differentially associated with auditory nerve and spinal trigeminal inputs to the cochlear nucleus** *J. Comp. Neurol* **500**:777–787 https://doi.org/10.1002/cne.21208

44. Liberman M.C. (1993) **Central projections of auditory nerve fibers of differing spontaneous rate, II: Posteroventral and dorsal cochlear nuclei** *J. Comp. Neurol* **327**:17–36 https://doi.org/10.1002/cne.903270103

45. Rouiller E.M., Cronin-Schreiber R., Fekete D.M., Ryugo D.K. (1986) **The central projections of intracellularly labeled auditory nerve fibers in cats: an analysis of terminal morphology** *J. Comp. Neurol* **249**:261–278 https://doi.org/10.1002/cne.902490210

46. Rouiller E.M., Ryugo D.K. (1984) **Intracellular marking of physiologically characterized cells in the ventral cochlear nucleus of the cat** *J. Comp. Neurol* **225**:167–186 https://doi.org/10.1002/cne.902250203

47. Tsuji J., Liberman M.C. (1997) **Intracellular labeling of auditory nerve fibers in guinea pig: central and peripheral projections** *J. Comp. Neurol* **381**:188–202 https://doi.org/10.1002/(SICI)1096-9861(19970505)381:2<188::AID-CNE6>3.0.CO;2-#

48. Liberman L.D., Wang H., Liberman M.C. (2011) **Opposing Gradients of Ribbon Size and AMPA Receptor Expression Underlie Sensitivity Differences among Cochlear-Nerve/Hair-Cell Synapses** *J. Neurosci* **31**:801–808 https://doi.org/10.1523/JNEURO-SCI.3389-10.2011

49. Liberman M.C. (1982) **Single-neuron labeling in the cat auditory nerve** *Science* **216**:1239–1241 https://doi.org/10.1126/sci-ence.7079757

50. Petitpré C. *et al.* (2018) **Neuronal heterogeneity and stereotyped connectivity in the auditory afferent system** *Nat. Commun* **9** https://doi.org/10.1038/s41467-018-06033-3

51. Shrestha B.R., Chia C., Wu L., Kujawa S.G., Liberman M.C., Goodrich L.V. (2018) **Sensory Neuron Diversity in the Inner Ear Is Shaped by Activity** *Cell* **174**:1229–1246 https://doi.org/10.1016/j.cell.2018.07.007

52. Siebald C., Vincent P.F.Y., Bottom R.T., Sun S., Reijntjes D.O.J., Manca M., Glowatzki E., Müller U. (2023) **Molecular signatures define subtypes of auditory afferents with distinct peripheral projection patterns and physiological properties** *Proc. Natl. Acad. Sci. U. S. A* **120** https://doi.org/10.1073/pnas.2217033120

53. Sun S., Babola T., Pregernig G., So K.S., Nguyen M., Su S.-S.M., Palermo A.T., Bergles D.E., Burns J.C., Müller U. (2018) **Hair Cell Mechanotransduction Regulates Spontaneous Activity and Spiral Ganglion Subtype Specification in the Auditory System** *Cell* **174**:1247–1263 https://doi.org/10.1016/j.cell.2018.07.008

54. Bolding K.A., Nagappan S., Han B.-X., Wang F., Franks K.M. (2020) **Recurrent circuitry is required to stabilize piriform cortex odor representations across brain states** *eLife* **9** https://doi.org/10.7554/eLife.53125

55. Muniak M.A., Rivas A., Montey K.L., May B.J., Francis H.W., Ryugo D.K. (2013) **3D model of frequency representation in the cochlear nucleus of the CBA/J mouse** *J. Comp. Neurol* **521**:1510–1532 https://doi.org/10.1002/cne.23238

56. Oertel D., Wu S.H., Garb M.W., Dizack C. (1990) **Morphology and physiology of cells in slice preparations of the posteroventral cochlear nucleus of mice** *J. Comp. Neurol* **295**:136–154 https://doi.org/10.1002/cne.902950112

57. Zhang Y.-P., Oertner T.G. (2007) **Optical induction of synaptic plasticity using a light-sensitive channel** *Nat. Methods* **4**:139–141 https://doi.org/10.1038/nmeth988

58. Jackman S.L., Beneduce B.M., Drew I.R., Regehr W.G. (2014) **Achieving High-Frequency Optical Control of Synaptic Transmission** *J. Neurosci* **34**:7704–7714 https://doi.org/10.1523/jneurosci.4694-13.2014

59. Oertel D., Bal R., Gardner S., PH (2000) **Detection of synchrony in the activity of auditory nerve fibers by octopus cells of the mammalian cochlear nucleus** *Proc. Of* **97**:11773–11779 https://doi.org/10.1073/pnas.97.22.1177397/22/11773

60. Cao X.J., Oertel D. (2010) **Auditory nerve fibers excite targets through synapses that vary in convergence, strength, and short-term plasticity** *J. Neurophysiol* **104**:2308–2320 https://doi.org/10.1152/jn.00451.2010

61. Cao X.-J., McGinley M.J., Oertel D. (2008) **Connections and synaptic function in the posteroventral cochlear nucleus of deaf jerker mice** *J. Comp. Neurol* **510**:297–308 https://doi.org/10.1002/cne.21788

62. Bal R., Baydas G., Naziroglu M. (2009) **Electrophysiological properties of ventral cochlear nucleus neurons of the dog** *Hear. Res* **256**:93–103 https://doi.org/10.1016/j.heares.2009.07.004

63. Lynch J.W., Rajendra S., Barry P.H., Schofield P.R. (1995) **Mutations Affecting the Glycine Receptor Agonist Transduction Mechanism Convert the Competitive Antagonist, Picrotoxin, into an Allosteric Potentiator** *J. Biol. Chem* **270**:13799–13806 https://doi.org/10.1074/jbc.270.23.13799

64. Pribilla I., Takagi T., Langosch D., Bormann J., Betz H. (1992) **The atypical M2 segment of the beta subunit confers picro-toxinin resistance to inhibitory glycine receptor channels** *EMBO J* **11**:4305–4311 https://doi.org/10.1002/j.1460-2075.1992.tb05529.x

65. Wang D.-S., Mangin J.-M., Moonen G., Rigo J.-M., Legen-dre P. (2006) **Mechanisms for Picrotoxin Block of α2 Homomeric Glycine Receptors** *J. Biol. Chem* **281**:3841–3855 https://doi.org/10.1074/jbc.M511022200

66. Hruskova B., Trojanova J., Kulik A., Kralikova M., Pysanenko K., Bures Z., Syka J., Trussell L.O., Turecek R. (2012) **Differential Distribution of Glycine Receptor Subtypes at the Rat Calyx of Held Synapse** *J. Neurosci* **32**:17012–17024 https://doi.org/10.1523/JNEUROSCI.1547-12.2012

67. Zhang X.-B., Sun G.-C., Liu L.-Y., Yu F., Xu T.-L. (2008) **Alpha2 subunit specificity of cyclothiazide inhibition on glycine receptors** *Mol. Pharmacol* **73**:1195–1202 https://doi.org/10.1124/mol.107.042655

68. Dutertre S., Becker C.-M., Betz H. (2012) **Inhibitory Glycine Receptors: An Update *** *J. Biol. Chem* **287**:40216–40223 https://doi.org/10.1074/jbc.R112.408229

69. Lynch J.W. (2009) **Native glycine receptor subtypes and their physiological roles** *Neuropharmacology* **56**:303–309 https://doi.org/10.1016/j.neuropharm.2008.07.034

70. Veruki M.L., Gill S.B., Hartveit E. (2007) **Spontaneous IP-SCs and glycine receptors with slow kinetics in wide-field amacrine cells in the mature rat retina** *J. Physiol* **581**:203–219 https://doi.org/10.1113/jphysiol.2006.127316

71. Manis P.B., Campagnola L. (2018) **A biophysical modelling platform of the cochlear nucleus and other auditory circuits: From channels to networks** *Hear. Res* **360**:76–91 https://doi.org/10.1016/j.heares.2017.12.017

72. Koch C., Poggio T., Torre V. (1983) **Nonlinear interactions in a dendritic tree: localization, timing, and role in information processing** *Proc. Natl. Acad. Sci. U. S. A* **80**:2799–2802

73. Hao J., Wang X., Dan Y., Poo M., Zhang X. (2009) **An arithmetic rule for spatial summation of excitatory and inhibitory inputs in pyramidal neurons** *Proc. Natl. Acad. Sci. U. S. A* **106**:21906–21911 https://doi.org/10.1073/pnas.0912022106

74. Moser T., Karagulyan N., Neef J., Jaime Tobón L.M. (2023) **Diversity matters — extending sound intensity coding by inner hair cells via heterogeneous synapses** *EMBO J* **42** https://doi.org/10.15252/embj.2023114587

75. Costalupes J.A., Young E.D., Gibson D.J. (1984) **Effects of continuous noise backgrounds on rate response of auditory nerve fibers in cat** *J. Neurophysiol* **51**:1326–1344 https://doi.org/10.1152/jn.1984.51.6.1326

76. Buran B.N., Strenzke N., Neef A., Gundelfinger E.D., Moser T., Liberman M.C. (2010) **Onset Coding Is Degraded in Auditory Nerve Fibers from Mutant Mice Lacking Synaptic Ribbons** *J. Neurosci* **30**:7587–7597 https://doi.org/10.1523/JNEUROSCI.0389-10.2010

77. Oliver D., Taberner A.M., Thurm H., Sausbier M., Arntz C., Ruth P., Fakler B., Liberman M.C. (2006) **The Role of BKCa Channels in Electrical Signal Encoding in the Mammalian Auditory Periphery** *J. Neurosci* **26**:6181–6189 https://doi.org/10.1523/JNEU-ROSCI.1047-06.2006

78. Bourien J., Tang Y., Batrel C., Huet A., Lenoir M., Ladrech S., Desmadryl G., Nouvian R., Puel J.-L., Wang J. (2014) **Contribution of auditory nerve fibers to compound action potential of the auditory nerve** *J. Neurophysiol* **112**:1025–1039 https://doi.org/10.1152/jn.00738.2013

79. McGinley M.J., Oertel D. (2006) **Rate thresholds determine the precision of temporal integration in principal cells of the ventral cochlear nucleus** *Hear. Res* :52–63 https://doi.org/10.1016/j.heares.2006.02.006

80. Zhang C., Wang M., Lin S., Xie R. (2022) **Calretinin-Expressing Synapses Show Improved Synaptic Efficacy with Reduced Asynchronous Release during High-Rate Activity** *J. Neurosci* **42**:2729–2742 https://doi.org/10.1523/JNEUROSCI.1773-21.2022

81. Huet A., Batrel C., Tang Y., Desmadryl G., Wang J., Puel J.-L., Bourien J. (2016) **Sound coding in the auditory nerve of ger-bils** *Hear. Res* **338**:32–39 https://doi.org/10.1016/j.heares.2016.05.006

82. Stasheff S.F., Masland R.H. (2002) **Functional Inhibition in Direction-Selective Retinal Ganglion Cells: Spatiotemporal Extent and Intralaminar Interactions** *J. Neurophysiol* **88**:1026–1039 https://doi.org/10.1152/jn.2002.88.2.1026

83. Ding H., Smith R.G., Poleg-Polsky A., Diamond J.S., Briggman K.L. (2016) **Species-specific wiring for direction selec-tivity in the mammalian retina** *Nature* **535**:105–110 https://doi.org/10.1038/nature18609

84. Bloss E.B., Cembrowski M.S., Karsh B., Colonell J., Fetter R.D., Spruston N. (2016) **Structured Dendritic Inhibition Supports Branch-Selective Integration in CA1 Pyramidal Cells** *Neuron* **89**:1016–1030 https://doi.org/10.1016/j.neuron.2016.01.029

85. Gidon A., Segev I. (2012) **Principles governing the operation of synaptic inhibition in dendrites** *Neuron* **75**:330–341 https://doi.org/10.1016/j.neuron.2012.05.015

86. Iascone D.M. *et al.* (2020) **Whole-Neuron Synaptic Mapping Reveals Spatially Precise Excitatory/In-hibitory Balance Limiting Dendritic and Somatic Spiking** *Neuron* **106**:566–578 https://doi.org/10.1016/j.neuron.2020.02.015

87. Jadi M., Polsky A., Schiller J., Mel B.W. (2012) **Location-Dependent Effects of Inhibition on Local Spiking in Pyramidal Neuron Dendrites** *PLOS Comput. Biol* **8** https://doi.org/10.1371/journal.pcbi.1002550

88. Lovett-Barron M., Turi G.F., Kaifosh P., Lee P.H., Bolze F., Sun X.-H., Nicoud J.-F., Zemelman B.V., Sternson S.M., Losonczy A. (2012) **Regulation of neuronal input transformations by tunable dendritic inhibition** *Nat. Neurosci* **15**:423–430 https://doi.org/10.1038/nn.3024

89. Bal R., Oertel D. (2007) **Voltage-activated calcium currents in octopus cells of the mouse cochlear nucleus** *JARO -J. Assoc. Res. Otolaryngol* **8**:509–521 https://doi.org/10.1007/s10162-007-0091-x

90. Cao X.-J., Oertel D. (2005) **Temperature Affects Voltage-Sensitive Conductances Differentially in Octopus Cells of the Mam-malian Cochlear Nucleus** *J. Neurophysiol* **94**:821–832 https://doi.org/10.1152/jn.01049.2004

91. Bal R., Baydas G. (2009) **Electrophysiological Properties of Octopus Neurons of the Cat Cochlear Nucleus: an In Vitro Study** *J. Assoc. Res. Otolaryngol* **10**:281–293 https://doi.org/10.1007/s10162-009-0159-x

92. Juiz J.M., Helfert R.H., Bonneau J.M., Wenthold R.J., Altschuler R.A. (1996) **Three classes of inhibitory amino acid terminals in the cochlear nucleus of the guinea pig** *J. Comp. Neurol* **373**:11–26 https://doi.org/10.1002/(SICI)1096-9861(19960909)373:1<11::AID-CNE2>3.0.CO;2-G

93. Kemmer M., Vater M. (1997) **The distribution of GABA and glycine immunostaining in the cochlear nucleus of the mustached bat (Pteronotus parnellii)** *Cell Tissue Res* **287**:487–506 https://doi.org/10.1007/s004410050773

94. Kolston J., Osen K.K., Hackney C.M., Ottersen O.P., Storm-Mathisen J. (1992) **An atlas of glycine-and GABA-like immunore-activity and colocalization in the cochlear nuclear complex of the guinea pig** *Anat. Embryol. (Berl* **186**:443–465

95. Moore J.K., Osen K.K., Storm-Mathisen J., Ottersen O.P. (1996) **gamma-Aminobutyric acid and glycine in the baboon coch-lear nuclei: an immunocytochemical colocalization study with reference to interspecies differences in inhibitory systems** *J. Comp. Neurol* **369**:497–519 https://doi.org/10.1002/(SICI)1096-9861(19960610)369:4<497::AID-CNE2>3.0.CO;2-#

96. Adams J.C., Mugnaini E. (1987) **Patterns of glutamate de-carboxylase immunostaining in the feline cochlear nuclear complex studied with silver enhancement and electron microscopy** *J. Comp. Neurol* **262**:375–401 https://doi.org/10.1002/cne.902620305

97. Friauf E., Hammerschmidt B., Kirsch J. (1997) **Development of adult-type inhibitory glycine receptors in the central auditory sys-tem of rats** *J. Comp. Neurol* **385**:117–134 https://doi.org/10.1002/(sici)1096-9861(19970818)385:1<117::aid-cne7>3.0.co;2-5

98. Sato K., Kuriyama H., Altschuler R.A. (2000) **Expression of glycine receptor subunit mRNAs in the rat cochlear nucleus** *Hear. Res* **144**:47–52 https://doi.org/10.1016/s0378-5955(00)00044-7

99. Schofield B.R., Cant N.B. (1996) **Origins and targets of commissural connections between the cochlear nuclei in guinea pigs** *J. Comp. Neurol* **375**:128–146 https://doi.org/10.1002/(SICI)1096-9861(19961104)375:1<128::AID-CNE8>3.0.CO;2-5

100. Thompson G.C., Cortez A.M., Lam D.M.K. (1985) **Localization of GABA immunoreactivity in the auditory brainstem of guinea pigs** *Brain Res* **339**:119–122 https://doi.org/10.1016/0006-8993(85)90628-6

101. Ngodup T., Romero G.E., Trussell L.O. (2020) **Identification of an inhibitory neuron subtype, the L-stellate cell of the cochlear nucleus** *eLife* **9** https://doi.org/10.7554/eLife.54350

102. Wickesberg R.E., Whitlon D., Oertel D. (1991) **Tubercu-loventral Neurons Project to the Multipolar Cell Area But Not to the Flexible Coincidence Detection in the Auditory System Octopus Cell Area of the Posteroventral Cochlear Nucleus** *J. Comp. Neurol.* **313**:457–468 https://doi.org/10.1002/cne.903130306

103. Kane E.S. (1977) **Descending inputs to octopus cell area of the cat cochlear nucleus: An electron microscopic study** *J. Comp. Neurol* **173**:337–354 https://doi.org/10.1002/cne.901730209

104. Felix R.A., Gourévitch B., Gómez-Álvarez M., Leijon S.C.M., Saldaña E., Magnusson A.K. (2017) **Octopus Cells in the Posteroventral Cochlear Nucleus Provide the Main Excitatory Input to the Superior Paraolivary Nucleus** *Front. Neural Circuits* **11**

105. Friauf E., Ostwald J. (1988) **Divergent projections of physio-logically characterized rat ventral cochlear nucleus neurons as shown by intra-axonal injection of horseradish peroxidase** *Exp. Brain Res* **73**:263–284 https://doi.org/10.1007/BF00248219

106. Schofield B.R. (1995) **Projections from the cochlear nucleus to the superior paraolivary nucleus in guinea pigs** *J. Comp. Neurol* **360**:135–149 https://doi.org/10.1002/cne.903600110

107. Thompson A.M., Thompson G.C. (1991) **Projections from the posteroventral cochlear nucleus to the superior olivary complex in guinea pig: Light and em observations with the PHA-L method** *J. Comp. Neurol* **311**:495–508 https://doi.org/10.1002/cne.903110405

108. Zook J.M., Casseday J.H. (1985) **Projections from the cochlear nuclei in the mustache bat, Pteronotus parnellii** *J. Comp. Neu-rol* **237**:307–324 https://doi.org/10.1002/cne.902370303

109. Adams J.C. (1997) **Projections from octopus cells of the posteroventral cochlear nucleus to the ventral nucleus of the lateral lemniscus in cat and human** *Audit. Neurosci* **3**:335–350

110. Berger C., Meyer E.M.M., Ammer J.J., Felmy F. (2014) **Large Somatic Synapses on Neurons in the Ventral Lateral Lem-niscus Work in Pairs** *J. Neurosci* **34**:3237–3246 https://doi.org/10.1523/JNEUROSCI.3664-13.2014

111. Nayagam D.A.X., Clarey J.C., Paolini A.G. (2005) **Powerful, Onset Inhibition in the Ventral Nucleus of the Lateral Lemniscus** *J. Neurophysiol* **94**:1651–1654 https://doi.org/10.1152/jn.00167.2005

112. Schofield B.R., Cant N.B. (1997) **Ventral nucleus of the lat-eral lemniscus in guinea pigs: Cytoarchitecture and inputs from the cochlear nucleus** *J. Comp. Neurol* **379**:363–385 https://doi.org/10.1002/(SICI)1096-9861(19970317)379:3<363::AID-CNE4>3.0.CO;2-1

113. Vater M., Feng A.S. (1990) **Functional organization of as-cending and descending connections of the cochlear nucleus of horseshoe bats** *J. Comp. Neurol* **292**:373–395 https://doi.org/10.1002/cne.902920305

114. Kawaguchi D., Sahara S., Zembrzycki A., O'Leary D.D.M. (2016) **Generation and analysis of an improved Foxg1-IRES-Cre driver mouse line** *Dev. Biol* **412**:139–147 https://doi.org/10.1016/j.ydbio.2016.02.011

115. Hatini V., Ye X., Balas G., Lai E. (1999) **Dynamics of plac-odal lineage development revealed by targeted transgene expression** *Dev. Dyn* **215**:332–343 https://doi.org/10.1002/(SICI)1097-0177(199908)215:4<332::AID-AJA5>3.0.CO;2-R

116. Pauley S., Lai E., Fritzsch B. (2006) **Foxg1 Is Required for Morphogenesis and Histogenesis of the Mammalian Inner Ear** *Dev. Dyn. Off. Publ. Am. Assoc. Anat* **235**:2470–2482 https://doi.org/10.1002/dvdy.20839

117. Hanashima C., Shen L., Li S.C., Lai E. (2002) **Brain Factor-1 Controls the Proliferation and Differentiation of Neocortical Pro-genitor Cells through Independent Mechanisms** *J. Neurosci* **22**:6526–6536 https://doi.org/10.1523/JNEUROSCI.22-15-06526.2002

118. Tao W., Lai E. (1992) **Telencephalon-restricted expression of BF-1, a new member of the HNF-3/fork head gene family, in the developing rat brain** *Neuron* **8**:957–966 https://doi.org/10.1016/0896-6273(92)90210-5

119. Miyoshi G., Fishell G. (2012) **Dynamic FoxG1 expression co-ordinates the integration of multipolar pyramidal neuron precursors into the cortical plate** *Neuron* **74**:1045–1058 https://doi.org/10.1016/j.neuron.2012.04.025

120. Lakso M., Pichel J.G., Gorman J.R., Sauer B., Okamoto Y., Lee E., Alt F.W., Westphal H. (1996) **Efficient in vivo manipulation of mouse genomic sequences at the zygote stage** *Proc. Natl. Acad. Sci. U. S. A* **93**:5860–5865 https://doi.org/10.1073/pnas.93.12.5860

121. Kakizaki T., Sakagami H., Sakimura K., Yanagawa Y. (2017) **A glycine transporter 2-Cre knock-in mouse line for gly-cinergic neuron-specific gene manipulation** *IBRO Rep* **3**:9–16 https://doi.org/10.1016/j.ibror.2017.07.002

122. Feng G., Mellor R.H., Bernstein M., Keller-Peck C., Nguyen Q.T., Wallace M., Nerbonne J.M., Lichtman J.W., Sanes J.R. (2000) **Imaging Neuronal Subsets in Transgenic Mice Ex-pressing Multiple Spectral Variants of GFP** *Neuron* **28**:41–51 https://doi.org/10.1016/S0896-6273(00)00084-2

123. Caberlotto E. *et al.* (2011) **Usher type 1G protein sans is a critical component of the tip-link complex, a structure controlling actin polymerization in stereocilia** *Proc. Natl. Acad. Sci. U. S. A* **108**:5825–5830 https://doi.org/10.1073/pnas.1017114108

124. Madisen L. *et al.* (2010) **A robust and high-throughput Cre reporting and characterization system for the whole mouse brain** *Nat. Neurosci* **13**:133–140 https://doi.org/10.1038/nn.2467

125. Sousa V.H., Miyoshi G., Hjerling-Leffler J., Karayannis T., Fishell G. (2009) **Characterization of Nkx6-2-derived neocortical interneuron lineages** *Cereb. Cortex N. Y. N 1991* **19**:i1–i10 https://doi.org/10.1093/cercor/bhp038

126. Madisen L. *et al.* (2012) **A toolbox of Cre-dependent optogenetic transgenic mice for light-in-duced activation and silencing** *Nat. Neurosci* **15**:793–802 https://doi.org/10.1038/nn.3078

127. Connelly C.J., Ryugo D.K., Muniak M.A. (2017) **The effect of progressive hearing loss on the morphology of endbulbs of Held and bushy cells** *Hear. Res* **343**:14–33 https://doi.org/10.1016/j.heares.2016.07.004

128. Susaki E.A., Tainaka K., Perrin D., Yukinaga H., Kuno A., Ueda H.R. (2015) **Advanced CUBIC protocols for whole-brain and whole-body clearing and imaging** *Nat. Protoc* **10**:1709–1727 https://doi.org/10.1038/nprot.2015.085

129. Matsumoto K. *et al.* (2019) **Advanced CUBIC tissue clearing for whole-organ cell profiling** *Nat. Protoc* **14**:3506–3537 https://doi.org/10.1038/s41596-019-0240-9

130. Rothman J.S., Silver R.A. (2018) **NeuroMatic: An Integrated Open-Source Software Toolkit for Acquisition, Analysis and Simulation of Electrophysiological Data** *Front. Neuroinformatics* **12** https://doi.org/10.3389/fninf.2018.00014

131. Hines M.L., Carnevale N.T. (1997) **The NEURON simulation environment** *Neural Comput* **9**:1179–1209 https://doi.org/10.1162/neco.1997.9.6.1179

Author information

Lauren J Kreeger
Harvard Medical School, Department of Neurobiology, Boston, USA

Suraj Honnuraiah
Harvard Medical School, Department of Neurobiology, Boston, USA, Stanley Center for Psychiatric Research, Broad Institute of MIT and Harvard, Cambridge, USA

Sydney Maeker
Harvard Medical School, Department of Neurobiology, Boston, USA

Siobhan Shea
Harvard Medical School, Department of Neurobiology, Boston, USA

Gord Fishell
Harvard Medical School, Department of Neurobiology, Boston, USA, Stanley Center for Psychiatric Research, Broad Institute of MIT and Harvard, Cambridge, USA

Lisa V Goodrich
Harvard Medical School, Department of Neurobiology, Boston, USA

For correspondence: lisa_goodrich@hms.harvard.edu

Editors

Reviewer #1 (Public review):

Kreeger and colleagues have explored the balance of excitation and inhibition in the cochlear nucleus octopus cells of mice using morphological, electrophysiological and computational methods. On the surface, the conclusion, that synaptic inhibition is present, does not seem like a leap. However, the octopus cells have been in the past portrayed as lacking synaptic inhibition. This view was supported by the paucity of glycinergic fibers in the octopus cell area and the lack of apparent IPSPs. Here, Kreeger et al., used beautiful immunohistochemical and mouse genetic methods to quantify the inhibitory and excitatory boutons over the complete surface of individual octopus cells and further analyzed the proportions of the different subtypes of spiral ganglion cell inputs. I think the analysis of synaptic distribution and the origin of the excitatory inputs stands as one of the most complete descriptions of any neuron, leaving little doubt about the presence of glycinergic boutons.

Kreeger et al then examined inhibition physiologically. Recordings from these neurons are notoriously difficult to make because of the enormous leak currents that shunt membrane stimuli and currents, and complicate voltage clamp. The authors have tried to overcome these limitations using drugs to block leak conductances, and computational approaches based on realistic parameters. They conclude that dendritic inhibition can modify the size and kinetics of excitatory signals, and may play out in computations made on temporally dispersed stimuli as might be experienced during a ramp in sound frequency or complex natural sounds like vocalizations.

https://doi.org/10.7554/eLife.100492.2.sa2

Reviewer #2 (Public review):

Kreeger et.al provided mechanistic evidence for flexible coincidence detection of auditory nerve synaptic inputs by octopus cells in the mouse cochlear nucleus. The octopus cells are highly specialized neurons that, with appropriate stimuli, can fire repetitively at very high rates (> 800 Hz in vivo), yield responses dominated by the onset of sound for simple stimuli, and integrate auditory nerve inputs over a wide frequency span. Previously, it was thought that octopus cells received little inhibitory input, and their integration of auditory input depended principally on temporally precise coincidence detection of excitatory auditory nerve inputs, coupled with a low input resistance established by high levels of expression of certain potassium channels and hyperpolarization-activated channels.

This study provides convincing evidence that octopus cells do in fact receive glycinergic synaptic input that can influence the efficacy of excitatory dendritic synaptic activity. By coupling selected genetic mouse models to characterize synaptic inputs and enable

optogenetic stimulation of subsets of afferents, fluorescent microscopy, detailed reconstructions of the location of inhibitory synapses on the soma and dendrites of octopus cells, slice physiology, and computational modeling, they have been able to clarify the presence of functional inhibition and elucidate some of the features of the inhibitory inputs to octopus cells at a biophysical level. They also show through modeling that inhibition is predicted to both provide shunting of synaptic currents and to change the peak timing of dendritic EPSPs as they travel to the soma. Both of these effects are potentially critically important in integration in these fast, coincidence-detecting neurons, and the magnitudes of the effects could have physiological significance. Overall, this work extends thinking about the functional sensory processing roles of octopus cells beyond the pre-existing hypotheses that are focussed primarily on the coincidence detection of excitatory inputs.

The authors have addressed all of my prior concerns, including improving several aspects of the presentation. The modeling is better described, which is critical because it provides a foundation to help interpret some of the physiology and to propose specific functions.

https://doi.org/10.7554/eLife.100492.2.sa1

Author response:

The following is the authors' response to the original reviews.

> ***eLife assessment***
>
> *This valuable work analyzes how specialized cells in the auditory cells, known as the octopus cells, can detect coincidences in their inputs at the submillisecond time scale. While previous work indicated that these cells receive no inhibitory inputs, the present study unambiguously demonstrates that these cells receive inhibitory glycinergic inputs. The physiologic impact of these inputs needs to be studied further. It remains incomplete at present but could be made solid by addressing caveats related to similar sizes of excitatory postsynaptic potentials and spikes in the octopus neurons.*

We apologize for not explicitly describing our experimental methods and analyses procedures that ensure the discrimination between action potentials and EPSPs. This has been addressed in responses to reviewer comments and amended in the manuscript.

> ***Reviewer #1 (Public Review):***
>
> *Kreeger and colleagues have explored the balance of excitation and inhibition in the cochlear nucleus octopus cells of mice using morphological, electrophysiological, and computational methods. On the surface, the conclusion, that synaptic inhibition is present, does not seem like a leap. However, the octopus cells have been in the past portrayed as devoid of inhibition. This view was supported by the seeming lack of glycinergic fibers in the octopus cell area and the lack of apparent IPSPs. Here, Kreeger et al. used beautiful immunohistochemical and mouse genetic methods to quantify the inhibitory and excitatory boutons over the complete surface of individual octopus cells and further analyzed the proportions of the different subtypes of spiral ganglion cell inputs. I think the analysis stands as one of the most complete descriptions of any neuron, leaving little doubt about the presence of glycinergic boutons.*
>
> *Kreeger et al then examined inhibition physiologically, but here I felt that the study was incomplete. Specifically, no attempt was made to assess the actual, biological values of synaptic conductance for AMPAR and GlyR. Thus, we don't really know how potent the GlyR could be in mediating inhibition. Here are some numbered comments:*

> *(1) "EPSPs" were evoked either optogenetically or with electrical stimulation. The resulting depolarizations are interpreted to be EPSPs. However previous studies from Oertel show that octopus cells have tiny spikes, and distinguishing them from EPSPs is tricky. No mention is made here about how or whether that was done. Thus, the analysis of EPSP amplitude is ambiguous.*

We agree that large EPSPs can be difficult to distinguish from an octopus cell's short spikes during experiments. During analysis, we distinguished spikes from EPSPs by generating phase plots, which allow us to visualize the first derivative of the voltage trace on the y-axis and the value of the voltage on the x-axis at each moment in time. In the example shown below, four depolarizing events were electrically evoked in an octopus cell (panel A). The largest of these events (shown in orange in panels B-D) has an amplitude of ~9mV and could be a small spike. The first derivative of the voltage (panel C) reveals a bi-phasic response in the larger orange trace, where during the rising phase (mV/ms > 0) of the EPSP there is a second, sharper rising phase for the spike. Like more traditionally sized action potentials, phase plots for octopus cell spikes also reveal a sharp change in the rate of voltage change over time (Author response image 1 panel D, ✱) after the rising action of the EPSP begins to slow. EPSPs (shown in blue in panels B-D) lack the deflection in the phase plot. Not all cases were as unambiguous as this example. Therefore, our analysis only included subthreshold stimulation that unambiguously evoked EPSPs, not spikes. A brief description of this analysis has been added to the methods text (lines 625-627) and we have noted in the results section that both ChR2-evoked and electrically-evoked stimulation can produce small action potentials, which were excluded from analysis (lines 156-158).

Author response image 1.

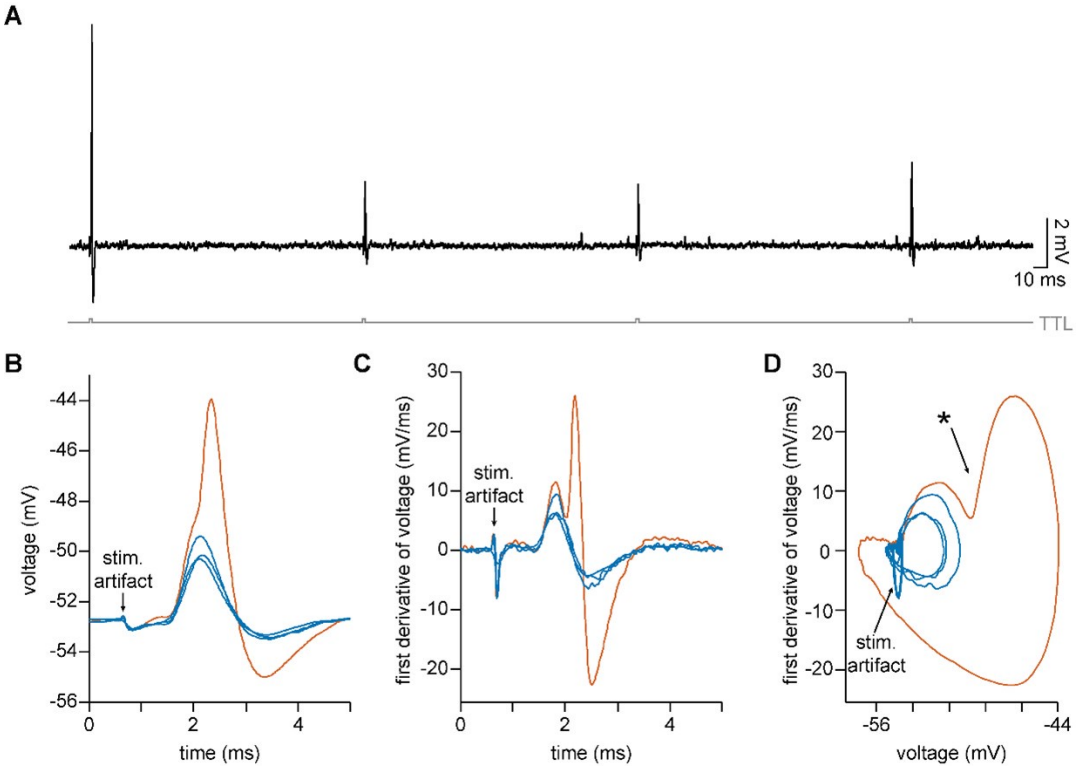

> *(2) For this and later analysis, a voltage clamp of synaptic inputs would have been a simple alternative to avoid contaminating spikes or shunts by background or voltage-gated conductances. Yet only the current clamp was employed. I can understand that the*

> *authors might feel that the voltage clamp is 'flawed' because of the failure to clamp dendrites. But that may have been a good price to pay in this case. The authors should have at least justified their choice of method and detailed its caveats.*

We agree that data collected using voltage-clamp would have eliminated the confound of short action potentials and avoided the influence of voltage-gated conductances. The large-diameter, and comparatively simple dendritic trees of octopus cells make them good morphological candidates for reliable voltage clamp. However, as suggested, we were concerned that the abundance of channels open at the neuron's resting potential would make it difficult to sufficiently clamp dendrites. Ultimately, given the low input resistances of octopus cells and the fast kinetics of excitatory inputs, we determined that bad voltage clamp conditions were likely to result in unclamped synaptic events with unpredicted distortions in kinetics and attenuation (To et al. 2022; PMID: 34480986; DOI: 10.1016/j.neuroscience.2021.08.024). We therefore chose to focus our efforts on current-clamp.

Beyond the limits of both current-clamp and voltage-clamp, we chose to leave all conductances that influence EPSP dendritic propagation intact because our model demonstrates that active Kv and leak conductances shape and attenuate synaptic inputs as they travel through the dendritic tree (Supp. Fig. 4F-G). The addition of voltage-clamp recordings would not impact the conclusions we make about EPSP summation at the soma. Future studies will need to focus on a dendrite-centric view of local excitatory and inhibitory summation. For dendrite-centric experiments, dendritic voltage-clamp recordings are well suited to answer that set of questions.

> *(3) The modeling raised several concerns. First, there is little presentation of assumptions, and of course, a model is entirely about its assumptions. For example, what excitatory conductance amplitudes were used? The same for inhibitory conductance? How were these values arrived at? The authors note that EPSGs and IPSGs had peaks at 0.3 and 3 ms. On what basis were these numbers obtained? The model's conclusions entirely depend on these values, and no measurements were made here that could have provided them. Parenthetical reference is made to Figure S5 where a range of values are tested, but with little explanation or justification.*

We apologize for not providing this information. We used our octopus neuron model to fit both EPSP and IPSP parameters to match experimental data. We have expanded the methods to include final values for the conductances (lines 649-651), which were adjusted to match experimental values seen in current-clamp recordings. We have also expanded the results section to describe each of the parameters we tuned (lines 203-222). An example of these adjustments is illustrated in Fig. 4F where the magnitude of inhibitory potentials at different conductances (100nS and 1nS) was compared to experimental data over a range of octopus cell input resistance conditions. Kinetic parameters were determined by aligning modeled PSPs to the rise times and full width at half maximum (FWHM) measurements from experiments under control and Kv block conditions. The experimental data for EPSPs and IPSPs that was used to fit the model is shown in Author response image 2 below.

Author response image 2.

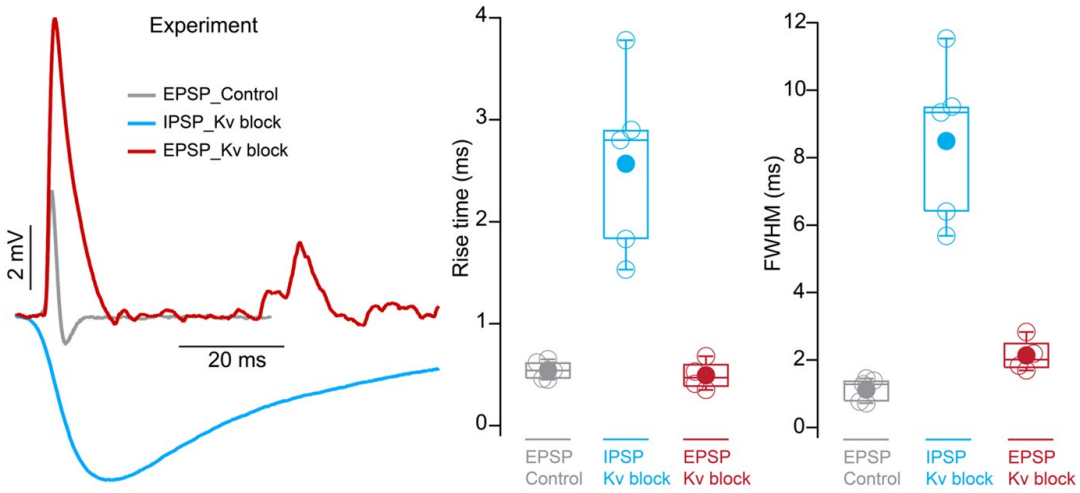

> *(4) In experiments that combined E and I stimulation, what exactly were time courses of the conductance changes, and how 'synchronous' were they, given the different methods to evoke them? (had the authors done voltage clamp they would know the answers).*

We chose to focus data collection on voltage changes at the soma under physiological conditions to better understand how excitation and inhibition integrate at the somatic compartment. Our conclusions in the combined E and I stimulation experiments require the resting membrane properties of octopus cells to be intact to make physiologically-relevant conclusions. Our current-clamp data includes the critical impact of leak, Kv, and HCN conductances on this computation. Reliable voltage-clamp would necessitate the removal of the Kv and HCN conductances that shape PSP magnitude, shape, and speed. Because it was not necessary to measure the conductances and kinetics of specific channels, we chose to use current-clamp.

Evoked IPSPs and EPSPs had cell-to-cell variability in their latencies to onset. Somatically-recorded optically-evoked inhibition under pharmacological conditions that changed cable properties had onset latencies between 2.5 and 4.3ms; electrically-evoked excitation under control conditions had latencies between 0.8 and 1.4ms. To overcome cell-to-cell timing variabilities, we presented a shuffled set of stimulation pairings that had a 3ms range of timings with 200µs intervals. As the evoked excitation and inhibition become more ‘synchronous’, the impact on EPSP magnitude and timing is greatest. Data presented in this paper was for the stimulation pairings that evokes a maximal shift in EPSP timing. On average, this occurred when the optical stimulation began ~1.2ms before electrical stimulation. Stimulation pairing times ranged between a 0ms offset and a 1.8ms offset at the extremes. An example of the shuffled stimulation pairings is shown in Author response image 3 below, and we have included information about the shuffled stimulus in the methods (lines 627-630)

Author response image 3.

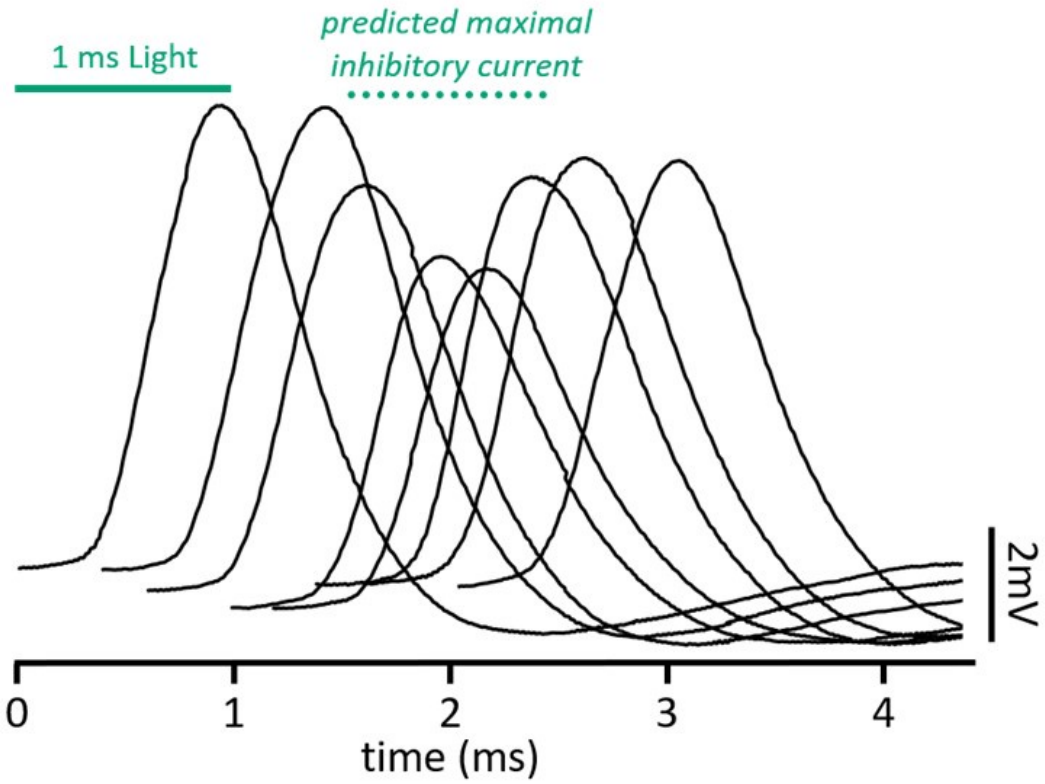

> *(5) Figure 4G is confusing to me. Its point, according to the text, is to show that changes in membrane properties induced by a block of Kv and HCN channels would not be expected to alter the amplitudes of EPSCs and IPSCs across the dendritic expanse. Now we are talking about currents (not shunting effects), and the presumption is that the blockers would alter the resting potential and thus the driving force for the currents. But what was the measured membrane potential change in the blockers? Surely that was documented. To me, the bigger concern (stated in the text) is whether the blockers altered exocytosis, and thus the increase in IPSP amplitude in blockers is due BOTH to loss of shunting and increase in presynaptic spike width. Added to this is that 4AP will reduce the spike threshold, thus allowing more ChR2-expressing axons to reach the threshold. Figure 4G does not address this point.*

These are valuable points that motivated us to improve the clarity of this figure and the corresponding text. We discussed two separate points in this paragraph and were not clear. Our intention with Figure 4G was to address concerns that using pharmacological blockers changes driving forces and may confound the measured change in magnitude of postsynaptic potentials. Membrane potentials hyperpolarized by approximately 8-10 mV after application of blockers. We corrected for this effect by adding a holding current to depolarize the neuron to its baseline resting potential. Text in the results (lines 187-190) and figure legends have been changed to clarify these points.

We also removed any discussion of presynaptic effects from this portion of the text because our description was incomplete and we did not directly collect data related to these claims. We originally wrote, “While blocking Kv and HCN allowed us to reveal IPSPs at the soma, 4-AP increases the duration of the already unphysiological ChR2-evoked presynaptic action

potential (Jackman et al., 2014; DOI: 10.1523/jneurosci.4694-13.2014), resulting in altered release probabilities and synaptic properties, amongst other caveats (Mathie et al., 1998; DOI: 10.1016/S0306-3623(97)00034-7)". Ultimately, effects on exocytosis, presynaptic excitability, or release probability are only relevant for the experiments presented in Figure 4. Figure 4 serves as evidence that synaptic release of glycine elicits strychnine-sensitive inhibitory postsynaptic potentials in octopus cells. Concerns of presynaptic effects do not carry over to the data presented in Figure 5, as Kv and HCN were not blocked in these experiments. Therefore, we have removed this portion of the text.

> *(6) Figure 5F is striking as the key piece of biological data that shows that inhibition does reduce the amplitude of "EPSPs" in octopus cells. Given the other uncertainties mentioned, I wondered if it makes sense as an example of shunting inhibition. Specifically, what are the relative synaptic conductances, and would you predict a 25% reduction given the actual (not modeled) values?*

We agree that both shunting and hyperpolarizing inhibition could play a role in the measured EPSP changes. Because we focused data collection on voltage changes at the soma under physiological conditions, we cannot calculate the relative synaptic conductances. Together, our experimental current-clamp results paired with estimates from the model provide compelling evidence for the change we observe in EPSPs. Regardless, the relative weights of the synaptic conductances is a very interesting question, but this information is not necessary to answer the questions posed in this study, namely the impact of dendritic inhibition on the arrival of EPSPs in the soma.

> *(7) Some of the supplemental figures, like 4 and 5, are hardly mentioned. Few will glean anything from them unless the authors direct attention to them and explain them better. In general, the readers would benefit from more complete explanations of what was done.*

We apologize for not fully discussing these figures in the results text. We have fully expanded the results section to detail the experiments and results presented in the supplement (lines 203-238).

> ***Reviewer #2 (Public Review):***
>
> *Summary:*
>
> *Kreeger et.al provided mechanistic evidence for flexible coincidence detection of auditory nerve synaptic inputs by octopus cells in the mouse cochlear nucleus. The octopus cells are specialized neurons that can fire repetitively at very high rates (> 800 Hz in vivo), yield responses dominated by the onset of sound for simple stimuli, and integrate auditory nerve inputs over a wide frequency span. Previously, it was thought that octopus cells received little inhibitory input, and their integration of auditory input depended principally on temporally precise coincidence detection of excitatory auditory nerve inputs, coupled with a low input resistance established by high levels of expression of certain potassium channels and hyperpolarization-activated channels.*
>
> *In this study, the authors used a combination of numerous genetic mouse models to characterize synaptic inputs and enable optogenetic stimulation of subsets of afferents, fluorescent microscopy, detailed reconstructions of the location of inhibitory synapses on the soma and dendrites of octopus cells, and computational modeling, to explore the importance of inhibitory inputs to the cells. They determined through assessment of excitatory and inhibitory synaptic densities that spiral ganglion neuron synapses are densest on the soma and proximal dendrite, while glycinergic inhibitory synaptic density is greater on the dendrites compared to the soma of octopus cells. Using different*

> *genetic lines, the authors further elucidated that the majority of excitatory synapses on the octopus cells are from type 1a spiral ganglion neurons, which have low response thresholds and high rates of spontaneous activity. In the second half of the paper, the authors employed electrophysiology to uncover the physiological response of octopus cells to excitatory and inhibitory inputs. Using a combination of pharmacological blockers in vitro cellular and computational modeling, the authors conclude that glycine in fact evokes IPSPs in octopus cells; these IPSPs are largely shunted by the high membrane conductance of the cells under normal conditions and thus were not clearly evident in prior studies. Pharmacological experiments point towards a specific glycine receptor subunit composition. Lastly, Kreeger et. al demonstrated with in vitro recordings and computational modeling that octopus cell inhibition modulates the amplitude and timing of dendritic spiral ganglion inputs to octopus cells, allowing for flexible coincidence detection.*
>
> *Strengths:*
>
> *The work combines a number of approaches and complementary observations to characterize the spatial patterns of excitatory and inhibitory synaptic input, and the type of auditory nerve input to the octopus cells. The combination of multiple mouse lines enables a better understanding of and helps to define, the pattern of synaptic convergence onto these cells. The electrophysiology provides excellent functional evidence for the presence of the inhibitory inputs, and the modeling helps to interpret the likely functional role of inhibition. The work is technically well done and adds an interesting dimension related to the processing of sound by these neurons. The paper is overall well written, the experimental tests are well-motivated and easy to follow. The discussion is reasonable and touches on both the potential implications of the work as well as some caveats.*
>
> *Weaknesses:*
>
> *While the conclusions presented by the authors are solid, a prominent question remains regarding the source of the glycinergic input onto octopus cells. In the discussion, the authors claim that there is no evidence for D-stellate, L-stellate, and tuberculoventral cell (all local inhibitory neurons of the ventral and dorsal cochlear nucleus) connections to octopus cells, and cite the relevant literature. An experimental approach will be necessary to properly rule out (or rule in) these cell types and others that may arise from other auditory brainstem nuclei. Understanding which cells provide the inhibitory input will be an essential step in clarifying its roles in the processing of sound by octopus cells.*

We are glad that the reviewer agrees with the conclusions we have made and is interested in learning more about how these findings impact sound processing. We agree that defining the source of inhibition will dramatically shape our understanding of the computation octopus cells are making. However, this is not an easy task, given the small size of the octopus cell area, and will involve considerable additional work. Since the overall findings do not depend on knowing the source of inhibition, we have instead re-written the discussion to clarify the lack of evidence for intrinsic inhibitory inputs to octopus cells, in addition to presenting likely candidates. As genetic profiles of cochlear nucleus and other auditory brainstem neurons become available, we intend to make and utilize genetic mouse models to answer questions like this.

> *The authors showed that type 1a SGNs are the most abundant inputs to octopus cells via microscopy. However, in Figure 3 they compare optical stimulation of all classes of ANFs, then compare this against stimulation of type 1b/c ANFs. While a difference in the paired-pulse ratio (and therefore, likely release probability) can be inferred by the difference*

> *between Foxg1-ChR2 and Ntng1-ChR2, it would have been preferable to have specific data with selective stimulation of type 1a neurons.*

We agree that complete genetic access to only the Ia population would have been the preferable approach, but we did not have an appropriate line when beginning these experiments. Because our results did not suggest a meaningful difference between the populations, we did not pursue further investigation once a line was available.

> ***Recommendations for the authors:***
>
> ***Reviewer #1 (Recommendations For The Authors):***
>
> *Besides the points mentioned in the main review:*
>
> *Minor*
>
> *(1) I really like the graphics and the immunohistological presentation.*
>
> *(2) Lines 316-319 say that octopus cells lack things like back-propagating spikes and dendritic Ca spikes. How do you know this?*

This statement was intended to be a summary of suggestions from the literature and lacked references and context as written. We have rewritten this section and clarified that our hypothesis was formed from data found in the literature (lines 334-337).

> *(3) Spectrograms of Figure 6A...where were these data obtained?*

We recorded and visualized human-generated rhythmic tapping and high-frequency squeaking sounds using Audacity. The visualizations of rhythmic tapping and imitated vocalizations are meant to show two different types of multi-frequency stimuli we hypothesize would result in somatic summation within an octopus cell's spike integration window, despite differences in timing. We rewrote the figure legend to explain more clearly what is shown and how it relates to the model in Figure 6.

> *(4) 'on-path' and 'off-path' seem like jargon that may not be clear to the average reader.*

Thank you for pointing out our use of unapproachable jargon. We have replaced the term from the figure with "proximal" and "distal" inhibition. In the main text, we now describe on-path and off-path together as the effect of location of dendritic inhibition on somatically recorded EPSPs.

> *(5) The paper could benefit from a table of modeled values.*

We have added specific details about the modelling in the text and clarified which modeled values were referenced from previous computational models and which were tuned to fit experimental data. Since most values were taken from a referenced publication, we did not add a table and instead point readers towards that source.

> *(6) Figure S4A-C what currents were delivered to the modeled cells?*

The model cells were injected with a -0.8 nA DC current for 300 ms in current clamp mode. This information has been added to the figure legend.

> *(7) In that figure "scaling factors" scale exactly which channels?*

Scaling factor is used to scale low-voltage activated K^+ ($\bar{g}_{KLT}$), high threshold K^+ ($\bar{g}_{KHT}$), fast transient K^+ ($\bar{g}_{KA}$), hyperpolarization-activated cyclic nucleotide-gated HCN ($\bar{g}_h$) but not fast Na^+ ($\bar{g}_{Na}$) and leak K^+ ($\bar{g}_{leak}$). This information has been added to the text (lines 205-208 and 646-653).

> *(8) In performing and modeling Kv/HCN block, do you know how complete the level of the block is?*

Since we cannot assess how complete the level of block is, we have changed the language in the text to clarify that we are reducing Kv and HCN channel conductance to the degree needed to increase resistance of the neuron (line 185).

> *(9) More on this Figure S4. It is hardly referred to in the text except to say that it supports that blocking the Kv/HCN channels will enhance the IPSP. Given how large the figure is, can you offer more of a conclusion than that? Also, in the synaptic model in that figure, the IPSCs are presumably happening in current-clamp conditions, and the reduction in amplitude of the IPSC (as opposed to the increase in IPSP) is due to hyperpolarization. Can you simply state that so readers can track what this figure is showing? Other similar things: what is a transfer impedance? How is it measured? What do we take from the analysis?*

We have elaborated on our description of both Supp. Fig. 4 and Supp. Fig. 5 in the results section of the text (lines 203-238).

> *(10) Figure S5 also needs a better explanation. E.g., in C-D, what does 'average' mean? The gray is an SD of this average? You modeled a range of values…but which ones are physiological? To me, this is a key point.*

We have elaborated on our description of both Supp. Fig. 4 and Supp. Fig. 5 in the results section of the text (lines 203-238).

> ***Reviewer #2 (Recommendations For The Authors):***
>
> *General:*
>
> *The images and 3-D reconstructions are visually stunning, but they are not colorblind-friendly and in some cases, hard to distinguish. This shows up particularly in the green and blue colors used in Figure 1. Also, better representative images could be used for Figure 1B.*

Thank you for pointing out that blue and green were difficult to distinguish in Figure 1H. We have outlined the green inhibitory puncta in this image to make them more distinguishable. We have also increased the resolution of the image in Figure 1B for better clarity. All other colors are selected from Wong, 2011 (PMID: 21850730; DOI: https://doi.org/10.1038/nmeth.1618).

> *Supplemental Figure 1D: The low-power view is good to have, but the CN is too small and the image appears a bit noisy. An inset showing the CN on a larger scale (higher resolution image?) would be more convincing. In this image, I see what appear to be cells in the DCN labeled, which calls into question the purity of the source of optogenetic synaptic activation. It is also difficult to tell whether there are other cells labeled in the VCN. Such inputs would still be minor, but it would be good to be very clear about the expression pattern.*

To offer more information about the activity of the *Ntng1*^{Cre} line in other regions of the auditory system, we increased the resolution of the image included in Supp. Fig. 1D and have also included an additional image (Supp. Fig. 1E) of a coronal section of the cochlear nucleus complex with *Ntng1*-tdT labelling. This image provides additional context for the cells labeled in the DCN. The text in the figure legend has been changed to clarify that some cells in the DCN were labeled (lines 118-120).

We agree that in the *Ntng1*^{Cre} experiments, there is the possibility of minor contamination from excitatory cells that express ChR2 outside of the spiral ganglion. This is also true for our *Foxg1*^{Cre} and *Foxg1*^{Flp} experiments, because these lines label cortical cells in addition to cochlear cells. However, we do not observe direct descending inputs from the cortex into the PVCN, making contamination from other *Foxg1*^{Cre}-positive neurons unlikely. While non-cochlear inputs from the *Ntng1*^{Cre} line are possible, evidence from both lines gives us confidence that we are not capturing inputs to octopus cells outside the cochlea. Central axons from Type I spiral ganglion neurons have VGLUT1+ synaptic terminals. When comparing the overlap between VGLUT1+ terminals and *Foxg1*-tdT labelling, we see full coverage. That is, all VGLUT+ terminals on octopus cells are co-labelled by *Foxg1*^{Cre}-mediated expression of tdTomato. An example image is shown below. Here, an octopus cell soma is labeled with blue fluorescent Nissl stain and inputs to the cochlear nucleus complex are labeled with *Foxg1*^{Cre}-dependent tdTomato (*Foxg1*-tdT; magenta). We have also immunolabeled for VGLUT1 puncta in green. This eliminates the possibility that VGLUT+ cells from outside the cochlea and cortex are sources of excitation to octopus cells.

Author response image 4.

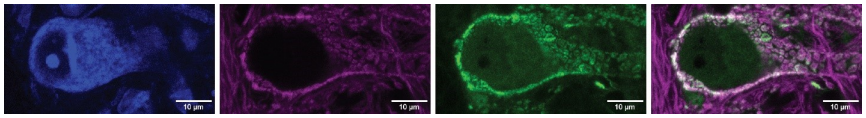

Further, we have looked at expression of *Ntng1*-tdT and *Foxg1*-EYFP together in the octopus cell area. An example image is shown below. All *Ntng1*-tdT+ fibers (magenta) are also *Foxg1*-EYFP+ (green), suggesting that all *Ntng1*^{Cre}-targeted inputs to octopus cells are a part of the *Foxg1*^{Cre}-targeted input population, which are very likely to only be from the cochlea. We have expanded the results section to include information about the overlap in expression driven by the *Ntng1*^{Cre} and *Foxg1*^{Flp} lines.

Author response image 5.

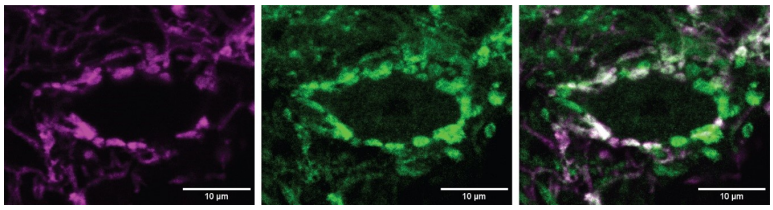

> *Supplemental Figure 2 G: These are a bit hard to read. Perhaps use a different image, or provide a reference outline drawing telling us what is what.*

We have used a different image with a Thy1-YFP labeled octopus cell for clarity.

> *In some places, the term "SGN" is used when referencing the axons and terminals within the CN, and without some context, this was occasionally confusing (SGN would seem to refer to the cell bodies). In some places in the text, it may be preferable to separate SGN, auditory nerve fibers (ANFs), and terminals, as entities for clarity.*

In order to make the study accessible to a broad neuroscience audience, we refer to the neurons of the spiral ganglion and their central axon projections using one name. We understand why, for those well acquainted with the auditory periphery, condensing terminology may feel awkward. However, for those readers unfamiliar with the anatomy of the cochlea and auditory nerve, we feel that the use of “SGN central axon” makes it clear that the “auditory nerve fibers” come from neurons in the spiral ganglion. This is clarified in the first paragraph of the introduction (lines 29-31) and in the methods (line 533).

> *Specific: Numbers refer to the line numbers on the manuscript.*
>
> *L29-31: Cochlear nucleus neurons are more general in their responses than this sentence indicates. While we can all agree that they are specialized to carry (or improve upon) the representation of these specific features of sound, they also respond more generally to sounds that might not have specific information in any of these domains. They are not silos of neural computation, and their outputs become mixed and "re-represented" well before they reach the auditory cortex. Octopus cells are no exception to this. I suggest striking most of the first paragraph, and instead using the first sentence to lead into the second paragraph, and putting the last sentence (of the current first paragraph) at the end of the second (now first) paragraph.*

We agree with this assessment and have made major changes to the introduction in line with these suggestions.

> *L33-46: A number of points in this paragraph need references (exp. line 41).*

We agree and have added references accordingly.

> *L43: Not sure what is meant by "fire at the onset of the sound, breaking it up into its frequency components"?*

We changed this text as part of a major reworking of the introduction.

> *L47-66: Again more citations are needed (at the end of sentence at line 55, probably moving some of the citations from the next sentence up).*

We agree and have added references accordingly.

> *L51: The consistent orientation of octopus cell dendrites across the ANFs has been claimed in the literature (as mentioned here), but there are some (perhaps problematic - plane of sectioning?) counterexamples from the older Golgi-stained images, and even amongst intracellularly stained cells (for example see Reccio-Spinoza and Rhode, 2020). This is important with regards to the broader hypothesis regarding traveling-wave compensation (e.g., McGinley et al; but also many others); if the cells are not all in the appropriate orientation then such compensation may be problematic. Likewise, the data from Lu et al., 2022, points towards a range of sensitivity to frequency-swept stimuli, some of which work in opposition to the traveling wave compensation hypothesis. It would seem that with the Thy1 mice, you have an opportunity to clarify the orientation. Figures 1A and 2A show a consistent dendritic orientation, assuming that these drawings*

> *are reconstructions of the cells as they were actually oriented in the tissue. Can you either comment on this or provide clearer evidence?*

We are happy to offer more information about the appearances of octopus cells in our preparations. In our hands, sparsely labeled octopus cells in Thy1-YFP-H mice show consistent dendritic orientation when visualized in a 15 degree parasaggital plane, with the most diversity apparent in cells with somas located more dorsally in the octopus cell area. We hypothesize that this is due to the limited area through which the central projections of spiral ganglion neurons (i.e. ANFs) must pass through before they enter the dorsal cochlear nucleus and continue their tonotopic organization in that area.

A caveat to studies without physiological or genetic identification of octopus cells is the assumption that all neurons in the octopus cell area are octopus cells. We find, especially along the borders of the octopus cell area, that stellate cells can be seen amongst octopus cells. Because stellate cell dendrites are not oriented like octopus cell dendrites, any stellate cells misidentified as octopus cells would appear to have poorly-oriented dendrites. This may explain why some studies report this finding. In addition, it can be difficult to assess tonotopic organization because of the 3D trajectory of tightly bundled axons, which is not capturable by a single section plane. Although a parasaggital plane of sectioning captures the tonotopic axis in one part of the octopus cell area, that same plane may be perpendicular at the opposing end.

> *L67: canonical -> exceptional.*

Thank you for the suggestion. We have made this change in the introduction.

> *L127: This paragraph was confusing on first reading. I don't think Supplemental Figure 1D shows the restricted pattern of expression very clearly. The "restricted to SGNs" might be better as "restricted to auditory nerve fibers" (except in the DCN, where there seem to be some scattered small cells?). A higher magnification image of the CN, but lower magnification than in panel E, would be helpful here.*

To avoid confusion, we have re-written this paragraph (lines 117-127) and included a higher magnification image of the CN in a revised Supp. Fig. 1.

> *L168: Here, perhaps say ANFs instead of SGNs.*

As above, we have decided to describe ANFs as SGN central axons to make the anatomy more accessible to people unfamiliar with cochlear anatomy.

> *L201-204: The IPSPs are surprisingly slow (Figures 5B, C), especially given the speed of the EPSPs/EPSCs in these cells. This is reminiscent of the asymmetry between EPSC and IPSC kinetics in bushy cells (Xie and Manis, 2014). The kinetics used in the model (3 ms; mentioned on line 624) however seem a bit arbitrary and no data is provided for the selection of that value. Were there any direct measurements of the IPSC kinetics (all of the traces in the paper are in the current clamp) that were used to justify this value?*

The kinetics of the somatically-recorded IPSPs are subject to the effects of our pharmacological manipulations. EPSPs measured at the soma under control conditions are small amplitude and rapid. With pharmacological reduction of HCN and Kv channels, EPSPs are larger and slower (please see figure in response to a similar question posed by Reviewer #1). We expect that this change also occurs with the IPSP kinetics under pharmacological conditions. Our justification of kinetics has been expanded and justified in the methods section (lines 641-661).

> *L594: Technically, this is a -11 mV junction potential, but thanks for including the information.*

We have corrected this in the text (line 618). Thank you for the close reading of all experimental and methodological details.

> *L595: The estimated power of the LED illumination at the focal plane should be measured and indicated here.*

We measured the power of the LED illumination at the focal plane using a PM100D Compact Power and Energy Meter Console (Thorlabs), a S120C Photodiode Power Sensor (Thorlabs), and a 1000µm diameter Circular Precision Pinhole (Thorlabs). Light intensity at the focal plane ranged between 1.9 and 4.1mW/mm^2, corresponding to 6% and 10% intensity on the Colibri5 system. We have reported these measurements in the results section (Lines 621-622).

> *L609: One concern about the model is that the integration time of 25 microseconds is rather close to the relative shifts in latency. While I doubt it will make a difference (except in the number), it may be worth verifying (spot checks, at least) that running the model with a 5 or 10-microsecond step yields a similar pattern of latency shifts (e.g., Supplementary Figure 5, Figure 5).*

Also, it is not clear what temperature the model was executed at (I would presume 35C); this needs to be given, and channel Q10's listed.

We realize that additional information is needed to fully understand the model and have added this to the results and the methods. The synaptic mechanism (.mod) files were obtained from Manis and Campagnola (2018) (PMID: 29331233; DOI: https://doi.org/10.1016/j.heares.2017.12.017). Q10 (3) and temperature (22°C) were also matched to parameters from Manis and Campagnola (2018). Because temperature is a critical factor for channel kinetics, we verified that our primary results remain consistent under conditions using a temperature of 35°C and a time step of 5µs, depicted below. Panel A illustrates the increase in IPSP as a function of glycine conductance under Kv+HCN block conditions at 35°C. As at 22°C, an increase in IPSP magnitude is absent in the control condition at 35°C. Panels B and C provide a direct comparison between the initial (i.e. 22°C) and suggested (i.e. 35°C) simulation conditions. Again we found that temperature does not have a major impact on the amplitude of IPSPs. Thus, results at 35°C do not change the conclusions we make from the model.

Author response image 6.

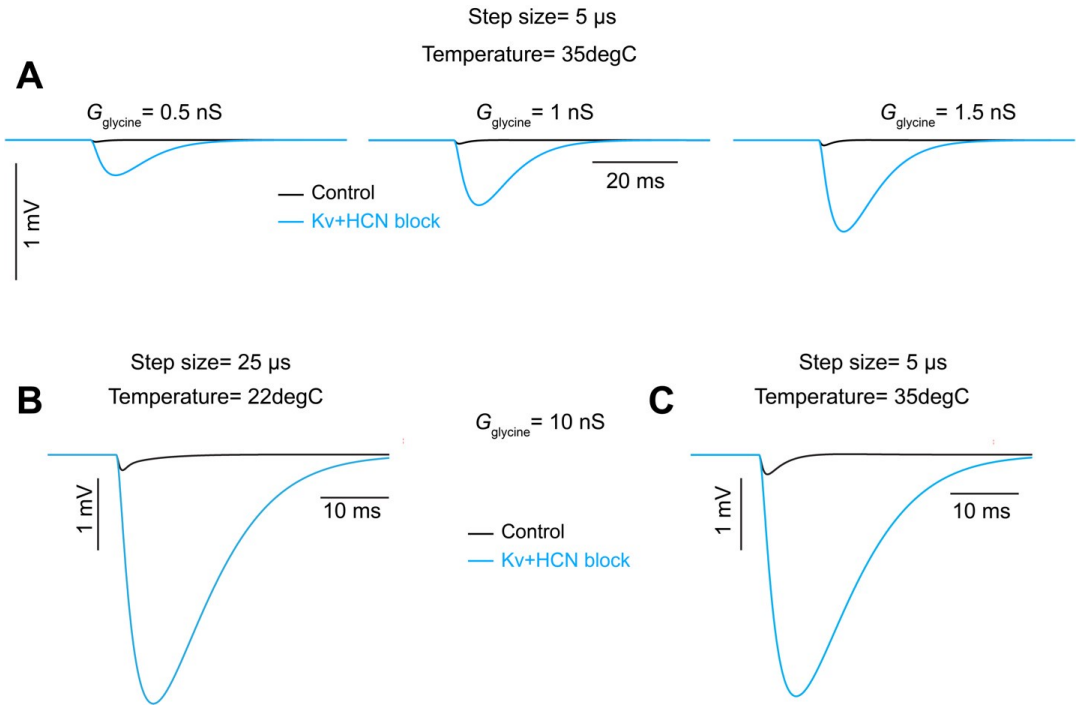

> *The nominal conductance densities should at least be provided in a table (supplemental, in addition to including them in the deposited code). The method for "optimization" of the conductance densities to match the experimental recordings needs to be described; the parameter space can be quite large in a model such as this. The McGinley reference needs a number.*

We added a more thorough description of modeling parameters and justification of choices in the methods section of the text (lines 641-661). We have also added a reference number to the McGinley 2012 reference in the text.

> *I think this is required by the journal:*
>
> *The model code, test results, and simulation results should be deposited in a public resource (Github would be preferable, but dryad, Zenodo, or Figshare could work), and the URL/doi for the resource provided in the manuscript. This includes the morphology swc/hoc file. The code should be in a form, and with a description, that readily allows an interested party with appropriate skills to download it and run it to generate the figures.*

We will upload the code and all associated simulation files to the ModelDB repository upon publication.

https://doi.org/10.7554/eLife.100492.2.sa0